2013) has evolved to be regulated by this dual-pronged post-translational control. mTORC2 regulates both mechanisms of FoxO-c-Myc axis regulation, and this nominates it as a critical metabolic regulator in cancer that must be suppressed, in addition to Akt, to abrogate c-Myc-dependent glycolysis and tumor growth.

EXPERIMENTAL PROCEDURES

Image Analysis-Based Scoring of Immunohistochemistry

Quantitative image analysis was performed with Soft Imaging System software (Olympus MicroSuite Analytical Suite). Representative images from each immunostained section were photographed using a Colorview II camera mounted on an Olympus BX61 microscope. Images were captured from representative regions of the tumor with sufficiently high tumor cell content based on hematoxylin and eosin staining evaluation. Borders between individual cells were approximated using a filter function. The amount of reaction product per cell was determined by measuring mean saturation per cell in the red-brown hue range. One thousand to fifteen hundred cells per case (on average) were measured for each marker. Negative control staining was also performed for each section without primary antibodies to determine the threshold for immunopositivity.

Tissue Microarray

TMA was constructed as reported previously (Guo et al., 2009), and immunohistochemical staining was performed as described previously (Choe et al., 2003; Lu et al., 2009) to analyze the expression of Ac-FoxO, c-Myc, p-NDRG1, and Rictor in 80 GBM samples and 26 normal brain samples. Cores were scored by a pathologist, and tumor staining intensity was compared to normal brain tissue.

Subcellular Fractionation and Electrophoretic Mobility Shift Assay

Nuclear fractionation was prepared from subconfluent 10 cm plates using a kit according to the manufacturer's instructions (Active Motif). Electrophoretic mobility shift assay (EMSA) was carried out using EMSA "Gel-Shift" Kit (Panomics). Nuclear extracts were incubated with a biotin-labeled oligonucleotide containing the consensus binding sequence for human FoxO (5′-CAAAACAA CAAAACAACAAAACAA-3′), and the transcription factor-bound oligonucleotide was separated from unbound oligonucleotide by electrophoresis on a 6% polyacrylamide gel. After being transferred to nylon membrane (GE Healthcare), the biotin-labeled bands were visualized using horseradish peroxidase-based chemiluminescence.

Mutagenesis

To generate the 5KR (using FoxO1) and 5KQ (using FoxO1 and FoxO1-AAA) mutants, we replaced the previously reported major acetylation sites, (van der Horst and Burgering, 2007; Zhao et al., 2010) K245, K248, K262, K265, and K274, with arginine or glutamine, respectively. To generate the 4KR mutant (using FoxO3), we replaced the acetylation sites (van der Horst and Burgering, 2007) K242, K259, K271, and K290 with arginine. We carried out site-directed mutagenesis using the QuikChange Kit (Stratagene).

Metabolite Measurements

Glucose, lactate, glutamine, and glutamate in the media of cultured cells were measured using the BioProfile Basic 4 analyzer (Nova Biomedical). Fresh media with 1% FBS were added to a 6-well plate of subconfluent cells, and metabolite concentration in the media was measured 24 hr later by comparison with blank media without cells and normalized to the number of cells in each well.

Real-Time RT-PCR and miRNA Studies

Total RNA was extracted by the use of RNeasy Plus Mini Kit (QIAGEN). First-strand cDNA was synthesized by the use of SuperScript III Transcriptase (Invitrogen). Real-time RT-PCR was performed with the iQ SYBR Green Supermix (Bio-Rad) on an iCycler (Bio-Rad) following the manufacturer's instructions. Primer sequences are available upon request. MicroRNAs were extracted by mirVana miRNA Isolation Kit (Applied Biosystems). MicroRNA reverse transcription was conducted by TaqMan MicroRNA Reverse Transcription Kit (Applied Biosystems), and miR-145, miR-34c, and RNU19 expression was detected by TaqMan MicroRNA Assays (Applied Biosystems). β-actin was used as an endogenous control for qRT-PCR, and RNU19 was used as an endogenous control for miRNA assays.

Glucose-Dependent Cell Proliferation and Cell Death Assay

Cells were placed in 96-well plates at 2.5×10^3 cells/well in 100 μl of growth medium and then incubated in each condition of treatment. For the measurement of glucose-dependent proliferation, DMEM containing glucose (Cellgro) or no-glucose DMEM (Gibco) supplemented with 4.5 g/l galactose (Sigma) was used as previously reported (Finley et al., 2011). Cell proliferation was examined with Cell Proliferation Assay Kit (Millpore) according to the manufacturer's instructions. The absorbance of the treated and untreated cells was measured with a microplate reader (Bio-Rad) at 420–480 nm. For the glucose-dependent cell death assay, cells were cultured with no-glucose DMEM + 10% FBS + galactose (4.5 g/l) or DMEM + 10% FBS + 2-Deoxy-D-glucose (2-DG, 10 mM) for 48 hr, and live/dead cells were quantified by cell counting with trypan blue exclusion and TC10 Automated Cell Counter (Bio-Rad). Data represent the mean ± SD of three independent experiments.

Animal Studies

TS516 tumor sphere lines originated from a GBM patient at Memorial Sloan-Kettering Cancer Center, or U87 and U87-EGFRvIII cell lines were implanted into immunodeficient SCID/Beige mice for subcutaneous xenograft studies. SCID/Beige mice were bred and kept under defined-flora pathogen-free conditions at the Association for Assessment of Laboratory Animal Care-approved Animal Facility of the Division of Experimental Radiation Oncology, UCLA. For subcutaneous implantation, exponentially growing tumor cells in culture were trypsinized, enumerated by trypan blue exclusion, and resuspended at 3×10^6 cells/ml in a solution of Dulbecco's phosphate-buffered saline and Matrigel (BD Biosciences). Tumor growth was monitored with calipers by measuring the perpendicular diameter of each subcutaneous tumor. Tumors were treated with a PI3K/mTOR dual inhibitor (XL765; 60 mg/kg) or normal saline every day for 19 days. Mice were euthanized if tumors reached 14 mm in maximum diameter or animals showed signs of illness. All experiments were conducted after approval by the Chancellor's Animal Research Committee of UCLA.

Statistical Analysis

Unpaired Student's t tests were performed unless otherwise noted. Error bars represented SEM unless otherwise noted, and statistical significance was indicated as $^*p < 0.05$, $^{**}p < 0.01$, and $^{***}p < 0.001$.

SUPPLEMENTAL INFORMATION

Supplemental Information includes five figures and Supplemental Experimental Procedures and can be found with this article online at http://dx.doi.org/10.1016/j.cmet.2013.09.013.

ACKNOWLEDGMENTS

We thank Dr. Cameron Brennan and Alicia Pedraza (Memorial Sloan-Kettering Cancer Center) for kindly giving us TS516 GBM sphere cell lines; Dr. Ciro Zanca, Tomoyuki Koga, John Anzola, and Yuki Ishii (Ludwig Institute for Cancer Research) for GBM6, GBM39, H1650, A549, and HeLa cell lines; and the UCLA Brain Tumor Translational Resource for biospecimen and biorepository support. A PI3K/mTOR dual inhibitor, XL765 (SAR245409), was kindly provided by Exelixis/Sanofi to I.K.M. This work is supported by grants from the National Institutes of Health (NS73831 and CA151819) (P.S.M.), NIH grant P01-CA95616 and a Fellow award from the National Foundation for Cancer Research (W.K.C.), and The Ben & Catherine Ivy Foundation and generous donations from the Ziering Family Foundation in memory of Sigi Ziering (T.F.C. and P.S.M.).

Received: May 13, 2013
Revised: July 25, 2013

Accepted: September 13, 2013
Published: October 17, 2013

REFERENCES

Albihn, A., Johnsen, J.I., and Henriksson, M.A. (2010). MYC in oncogenesis and as a target for cancer therapies. Adv. Cancer Res. *107*, 163–224.

Babic, I., Anderson, E.S., Tanaka, K., Guo, D., Masui, K., Li, B., Zhu, S., Gu, Y., Villa, G.R., Akhavan, D., et al. (2013). EGFR mutation-induced alternative splicing of Max contributes to growth of glycolytic tumors in brain cancer. Cell Metab. *17*, 1000–1008.

Bensaad, K., Tsuruta, A., Selak, M.A., Vidal, M.N., Nakano, K., Bartrons, R., Gottlieb, E., and Vousden, K.H. (2006). TIGAR, a p53-inducible regulator of glycolysis and apoptosis. Cell *126*, 107–120.

Biggs, W.H., 3rd, Meisenhelder, J., Hunter, T., Cavenee, W.K., and Arden, K.C. (1999). Protein kinase B/Akt-mediated phosphorylation promotes nuclear exclusion of the winged helix transcription factor FKHR1. Proc. Natl. Acad. Sci. USA *96*, 7421–7426.

Bouchard, C., Marquardt, J., Brás, A., Medema, R.H., and Eilers, M. (2004). Myc-induced proliferation and transformation require Akt-mediated phosphorylation of FoxO proteins. EMBO J. *23*, 2830–2840.

Brunet, A., Sweeney, L.B., Sturgill, J.F., Chua, K.F., Greer, P.L., Lin, Y., Tran, H., Ross, S.E., Mostoslavsky, R., Cohen, H.Y., et al. (2004). Stress-dependent regulation of FOXO transcription factors by the SIRT1 deacetylase. Science *303*, 2011–2015.

Cairns, R.A., Harris, I.S., and Mak, T.W. (2011). Regulation of cancer cell metabolism. Nat. Rev. Cancer *11*, 85–95.

Cancer Genome Atlas Research Network. (2008). Comprehensive genomic characterization defines human glioblastoma genes and core pathways. Nature *455*, 1061–1068.

Choe, G., Horvath, S., Cloughesy, T.F., Crosby, K., Seligson, D., Palotie, A., Inge, L., Smith, B.L., Sawyers, C.L., and Mischel, P.S. (2003). Analysis of the phosphatidylinositol 3′-kinase signaling pathway in glioblastoma patients in vivo. Cancer Res. *63*, 2742–2746.

Christofk, H.R., Vander Heiden, M.G., Wu, N., Asara, J.M., and Cantley, L.C. (2008). Pyruvate kinase M2 is a phosphotyrosine-binding protein. Nature *452*, 181–186.

Dang, C.V. (2012a). MYC on the path to cancer. Cell *149*, 22–35.

Dang, C.V. (2012b). Links between metabolism and cancer. Genes Dev. *26*, 877–890.

Dang, C.V., Le, A., and Gao, P. (2009). MYC-induced cancer cell energy metabolism and therapeutic opportunities. Clin. Cancer Res. *15*, 6479–6483.

DeBerardinis, R.J., Lum, J.J., Hatzivassiliou, G., and Thompson, C.B. (2008). The biology of cancer: metabolic reprogramming fuels cell growth and proliferation. Cell Metab. *7*, 11–20.

Delpuech, O., Griffiths, B., East, P., Essafi, A., Lam, E.W., Burgering, B., Downward, J., and Schulze, A. (2007). Induction of Mxi1-SR alpha by FOXO3a contributes to repression of Myc-dependent gene expression. Mol. Cell. Biol. *27*, 4917–4930.

Faubert, B., Boily, G., Izreig, S., Griss, T., Samborska, B., Dong, Z., Dupuy, F., Chambers, C., Fuerth, B.J., Viollet, B., et al. (2013). AMPK is a negative regulator of the Warburg effect and suppresses tumor growth in vivo. Cell Metab. *17*, 113–124.

Ferber, E.C., Peck, B., Delpuech, O., Bell, G.P., East, P., and Schulze, A. (2012). FOXO3a regulates reactive oxygen metabolism by inhibiting mitochondrial gene expression. Cell Death Differ. *19*, 968–979.

Finley, L.W., Carracedo, A., Lee, J., Souza, A., Egia, A., Zhang, J., Teruya-Feldstein, J., Moreira, P.I., Cardoso, S.M., Clish, C.B., et al. (2011). SIRT3 opposes reprogramming of cancer cell metabolism through HIF1α destabilization. Cancer Cell *19*, 416–428.

Gan, B., Lim, C., Chu, G., Hua, S., Ding, Z., Collins, M., Hu, J., Jiang, S., Fletcher-Sananikone, E., Zhuang, L., et al. (2010). FoxOs enforce a progression checkpoint to constrain mTORC1-activated renal tumorigenesis. Cancer Cell *18*, 472–484.

Guertin, D.A., Stevens, D.M., Thoreen, C.C., Burds, A.A., Kalaany, N.Y., Moffat, J., Brown, M., Fitzgerald, K.J., and Sabatini, D.M. (2006). Ablation in mice of the mTORC components raptor, rictor, or mLST8 reveals that mTORC2 is required for signaling to Akt-FOXO and PKCalpha, but not S6K1. Dev. Cell *11*, 859–871.

Guo, D., Hildebrandt, I.J., Prins, R.M., Soto, H., Mazzotta, M.M., Dang, J., Czernin, J., Shyy, J.Y., Watson, A.D., Phelps, M., et al. (2009). The AMPK agonist AICAR inhibits the growth of EGFRvIII-expressing glioblastomas by inhibiting lipogenesis. Proc. Natl. Acad. Sci. USA *106*, 12932–12937.

Hagiwara, A., Cornu, M., Cybulski, N., Polak, P., Betz, C., Trapani, F., Terracciano, L., Heim, M.H., Rüegg, M.A., and Hall, M.N. (2012). Hepatic mTORC2 activates glycolysis and lipogenesis through Akt, glucokinase, and SREBP1c. Cell Metab. *15*, 725–738.

Hudson, C.C., Liu, M., Chiang, G.G., Otterness, D.M., Loomis, D.C., Kaper, F., Giaccia, A.J., and Abraham, R.T. (2002). Regulation of hypoxia-inducible factor 1alpha expression and function by the mammalian target of rapamycin. Mol. Cell. Biol. *22*, 7004–7014.

Ilic, N., Utermark, T., Widlund, H.R., and Roberts, T.M. (2011). PI3K-targeted therapy can be evaded by gene amplification along the MYC-eukaryotic translation initiation factor 4E (eIF4E) axis. Proc. Natl. Acad. Sci. USA *108*, E699–E708.

Kaelin, W.G., Jr., and Ratcliffe, P.J. (2008). Oxygen sensing by metazoans: the central role of the HIF hydroxylase pathway. Mol. Cell *30*, 393–402.

Koppenol, W.H., Bounds, P.L., and Dang, C.V. (2011). Otto Warburg's contributions to current concepts of cancer metabolism. Nat. Rev. Cancer *11*, 325–337.

Kress, T.R., Cannell, I.G., Brenkman, A.B., Samans, B., Gaestel, M., Roepman, P., Burgering, B.M., Bushell, M., Rosenwald, A., and Eilers, M. (2011). The MK5/PRAK kinase and Myc form a negative feedback loop that is disrupted during colorectal tumorigenesis. Mol. Cell *41*, 445–457.

Levine, A.J., and Puzio-Kuter, A.M. (2010). The control of the metabolic switch in cancers by oncogenes and tumor suppressor genes. Science *330*, 1340–1344.

Liu, J., and Levens, D. (2006). Making myc. Curr. Top. Microbiol. Immunol. *302*, 1–32.

Lu, K.V., Zhu, S., Cvrljevic, A., Huang, T.T., Sarkaria, S., Ahkavan, D., Dang, J., Dinca, E.B., Plaisier, S.B., Oderberg, I., et al. (2009). Fyn and SRC are effectors of oncogenic epidermal growth factor receptor signaling in glioblastoma patients. Cancer Res. *69*, 6889–6898.

Marroquin, L.D., Hynes, J., Dykens, J.A., Jamieson, J.D., and Will, Y. (2007). Circumventing the Crabtree effect: replacing media glucose with galactose increases susceptibility of HepG2 cells to mitochondrial toxicants. Toxicol. Sci. *97*, 539–547.

Mihaylova, M.M., Vasquez, D.S., Ravnskjaer, K., Denechaud, P.D., Yu, R.T., Alvarez, J.G., Downes, M., Evans, R.M., Montminy, M., and Shaw, R.J. (2011). Class IIa histone deacetylases are hormone-activated regulators of FOXO and mammalian glucose homeostasis. Cell *145*, 607–621.

Muellner, M.K., Uras, I.Z., Gapp, B.V., Kerzendorfer, C., Smida, M., Lechtermann, H., Craig-Mueller, N., Colinge, J., Duernberger, G., and Nijman, S.M. (2011). A chemical-genetic screen reveals a mechanism of resistance to PI3K inhibitors in cancer. Nat. Chem. Biol. *7*, 787–793.

Nakamura, N., Ramaswamy, S., Vazquez, F., Signoretti, S., Loda, M., and Sellers, W.R. (2000). Forkhead transcription factors are critical effectors of cell death and cell cycle arrest downstream of PTEN. Mol. Cell. Biol. *20*, 8969–8982.

Peck, B., Ferber, E.C., and Schulze, A. (2013). Antagonism between FOXO and MYC Regulates Cellular Powerhouse. Front Oncol. *3*, 96.

Plas, D.R., and Thompson, C.B. (2005). Akt-dependent transformation: there is more to growth than just surviving. Oncogene *24*, 7435–7442.

Potthoff, M.J., Wu, H., Arnold, M.A., Shelton, J.M., Backs, J., McAnally, J., Richardson, J.A., Bassel-Duby, R., and Olson, E.N. (2007). Histone deacetylase degradation and MEF2 activation promote the formation of slow-twitch myofibers. J. Clin. Invest. *117*, 2459–2467.

Rohle, D., Popovici-Muller, J., Palaskas, N., Turcan, S., Grommes, C., Campos, C., Tsoi, J., Clark, O., Oldrini, B., Komisopoulou, E., et al. (2013). An inhibitor of mutant IDH1 delays growth and promotes differentiation of glioma cells. Science *340*, 626–630.

Tanaka, K., Babic, I., Nathanson, D., Akhavan, D., Guo, D., Gini, B., Dang, J., Zhu, S., Yang, H., De Jesus, J., et al. (2011). Oncogenic EGFR signaling activates an mTORC2-NF-κB pathway that promotes chemotherapy resistance. Cancer Discov. *1*, 524–538.

Tong, X., Zhao, F., and Thompson, C.B. (2009). The molecular determinants of de novo nucleotide biosynthesis in cancer cells. Curr. Opin. Genet. Dev. *19*, 32–37.

van der Horst, A., and Burgering, B.M. (2007). Stressing the role of FoxO proteins in lifespan and disease. Nat. Rev. Mol. Cell Biol. *8*, 440–450.

Vander Heiden, M.G., Cantley, L.C., and Thompson, C.B. (2009). Understanding the Warburg effect: the metabolic requirements of cell proliferation. Science *324*, 1029–1033.

Wang, B., Moya, N., Niessen, S., Hoover, H., Mihaylova, M.M., Shaw, R.J., Yates, J.R., 3rd, Fischer, W.H., Thomas, J.B., and Montminy, M. (2011). A hormone-dependent module regulating energy balance. Cell *145*, 596–606.

Warburg, O. (1956). On the origin of cancer cells. Science *123*, 309–314.

Ward, P.S., and Thompson, C.B. (2012). Metabolic reprogramming: a cancer hallmark even warburg did not anticipate. Cancer Cell *21*, 297–308.

Zhao, Y., Yang, J., Liao, W., Liu, X., Zhang, H., Wang, S., Wang, D., Feng, J., Yu, L., and Zhu, W.G. (2010). Cytosolic FoxO1 is essential for the induction of autophagy and tumour suppressor activity. Nat. Cell Biol. *12*, 665–675.

Zhao, Y., Wang, Y., and Zhu, W.G. (2011). Applications of post-translational modifications of FoxO family proteins in biological functions. J. Mol. Cell Biol. *3*, 276–282.

PML mediates glioblastoma resistance to mammalian target of rapamycin (mTOR)-targeted therapies

Akio Iwanami[a], Beatrice Gini[b,c,1], Ciro Zanca[b,1], Tomoo Matsutani[b], Alvaro Assuncao[d], Ali Nael[e], Julie Dang[f], Huijun Yang[b], Shaojun Zhu[g], Jun Kohyama[g], Issay Kitabayashi[h], Webster K. Cavenee[b,i], Timothy F. Cloughesy[j], Frank B. Furnari[b,i,k], Masaya Nakamura[a], Yoshiaki Toyama[a], Hideyuki Okano[l], and Paul S. Mischel[b,i,k,2]

Departments of [a]Orthopaedic Surgery and [l]Physiology, Keio University School of Medicine, Tokyo 160-8582, Japan; [b]Ludwig Institute for Cancer Research, [i]Moores Comprehensive Cancer Center, and [k]Department of Pathology, University of California at San Diego, La Jolla, CA 92093; [c]Department of Neurological, Neuropsychological, Morphological and Movement Sciences, University of Verona, 37134 Verona, Italy; [d]Undergraduate Minor in Biomedical Research Program, and Departments of [g]Molecular and Medical Pharmacology and [j]Neurology, University of California, Los Angeles, CA 90095; [e]Department of Pathology, University of California, Irvine, CA 92697; [f]School of Pharmacy, University of California, San Francisco, CA 94104; and [h]Division of Hematological Malignancy, National Cancer Center Research Institute, Tokyo 104-0045, Japan

Edited[†] by Joseph Schlessinger, Yale University School of Medicine, New Haven, CT, and approved February 1, 2013 (received for review October 12, 2012)

Despite their nearly universal activation of mammalian target of rapamycin (mTOR) signaling, glioblastomas (GBMs) are strikingly resistant to mTOR-targeted therapy. We analyzed GBM cell lines, patient-derived tumor cell cultures, and clinical samples from patients in phase 1 clinical trials, and find that the promyelocytic leukemia (PML) gene mediates resistance to mTOR-targeted therapies. Direct mTOR inhibitors and EGF receptor (EGFR) inhibitors that block downstream mTOR signaling promote nuclear PML expression in GBMs, and genetic overexpression and knockdown approaches demonstrate that PML prevents mTOR and EGFR inhibitor-dependent cell death. Low doses of the PML inhibitor, arsenic trioxide, abrogate PML expression and reverse mTOR kinase inhibitor resistance in vivo, thus markedly inhibiting tumor growth and promoting tumor cell death in mice. These results identify a unique role for PML in mTOR and EGFR inhibitor resistance and provide a strong rationale for a combination therapeutic strategy to overcome it.

mTORC1 | glioma

Glioblastoma (GBM) is the most common malignant primary brain tumor of adults and one of the most lethal forms of cancer (1, 2). As a consequence of frequent EGF receptor (EGFR) amplification and/or activating mutation, other receptor tyrosine kinase amplifications and phosphatase and tensin homolog (PTEN) loss (3, 4), persistent hyperactivation of the phosphatidyl-inositol-3-kinase (PI3K) pathway is observed in nearly 90% of GBMs making the downstream effector, mammalian target of rapamycin (mTOR), a compelling drug target. mTOR links growth factor signaling through PI3K to energy and nutrient status, protein translation, autophagy, and tumor cell metabolism (5). Thus, mTOR is a critical integrator that regulates tumor growth, survival and, potentially, cancer drug resistance.

The allosteric mTOR inhibitor rapamycin has failed in the clinic as a treatment for GBM patients. We previously reported that in a clinical phase I trial for patients with recurrent PTEN-deficient GBM, rapamycin treatment led to Akt activation resulting in loss of negative feedback, consistent with the homeostatic regulatory role of mTOR complex I (mTORC1) as a negative regulator of PI3K/Akt signaling (6). Further, we demonstrated a critical role for mTOR complex II (mTORC2) as a critical mediator of rapamycin resistance through Akt and mTORC1-independent signaling pathways (7). These results have highlighted the potential role for mTOR kinase inhibitors, which block both mTOR signaling complexes, in the treatment of GBM and potentially other cancers.

The interconnectivity between mTOR signaling complexes suggests the possibility that multiple mechanisms of mTOR inhibitor resistance may exist, some of which may be clinically actionable. The promyelocytic leukemia (PML) gene may represent one such mechanism. PML is a pleiotropic tumor suppressor that plays multiple roles on cellular homeostasis such as apoptosis, proliferation, and senescence (8, 9). PML, as part of the retinoic acid receptor (RAR)/PML fusion protein identified in acute promyelocytic leukemia, represents one of the first molecular cancer targets amenable to targeted drug therapy (10, 11). Although the loss of PML protein expression is associated with tumor progression in many tumors (12), some tumors show paradoxically high levels of PML. For example, PML has been shown to be highly expressed in hematopoetic stem cells and in chemotherapy resistant, quiescent leukemia-initiating CML cells (13).

PML is also closely related to receptor tyrosine kinase (RTK)/PI3K/Akt/mTOR signaling pathway at multiple levels. PML has been reported to oppose the function of nuclear Akt (14) and was also identified as a repressor of mTOR through inhibition of Ras homolog enriched in brain (Rheb)–mTOR interaction during hypoxia (15). Further, PML is responsible for the repression of transcriptional activity from the EGFR promoter (16). Considering these factors, we hypothesized that PML might promote resistance to rapamycin, ATP-competitive mTOR kinase inhibitors, and EGFR tyrosine kinase inhibitors by controlling RTK/PI3K/Akt/mTOR signaling and cell cycle in GBM. Here, we examine the expression of PML in GBM cell lines and GBM-patient tissues; show that it is regulated by PI3K/Akt/mTOR signaling; demonstrate the impact of mTOR inhibition on PML expression; and then, using genetic and pharmacological approaches and correlations from clinical samples of patients treated with rapamycin or erlotinib, demonstrate a role for PML in preventing drug-induced apopotosis and promoting clinical resistance. Finally, we identify genetic and pharmacological approaches to overcome this drug resistance.

Results

PML Expression in GBM Patients. To examine the expression of PML in GBM patients, we performed immunohistochemical analysis of GBM by using a tissue microarray (TMA) consisting of multiple representative regions of tumor and adjacent normal tissue from 87 patients with primary GBMs (17, 18). Expression of PML, Ki-67, and phospho-S6 was analyzed and scored independently by two neuropathologists as high or low (scoring summarized in Fig. 1 *A* and *B*). PML was highly expressed in 41.4% of tumor samples (Fig. 1 *A* and *B*), and the expression was

Author contributions: A.I., B.G., C.Z., W.K.C., T.F.C., F.B.F., and P.S.M. designed research; A.I., B.G., C.Z., T.M., A.A., A.N., J.D., H.Y., S.Z., and J.K. performed research; C.Z., T.M., I.K., and F.B.F. contributed new reagents/analytic tools; A.I., B.G., C.Z., T.M., W.K.C., T.F.C., F.B.F., M.N., Y.T., H.O., and P.S.M. analyzed data; and A.I., B.G., C.Z., T.M., W.K.C., T.F.C., F.B.F., M.N., Y.T., H.O., and P.S.M. wrote the paper.

The authors declare no conflict of interest.

[†]This Direct Submission article had a prearranged editor.

Freely available online through the PNAS open access option.

[1]B.G. and C.Z. contributed equally to this work.

[2]To whom correspondence should be addressed. E-mail: pmischel@ucsd.edu.

This article contains supporting information online at www.pnas.org/lookup/suppl/doi:10.1073/pnas.1217602110/-/DCSupplemental.

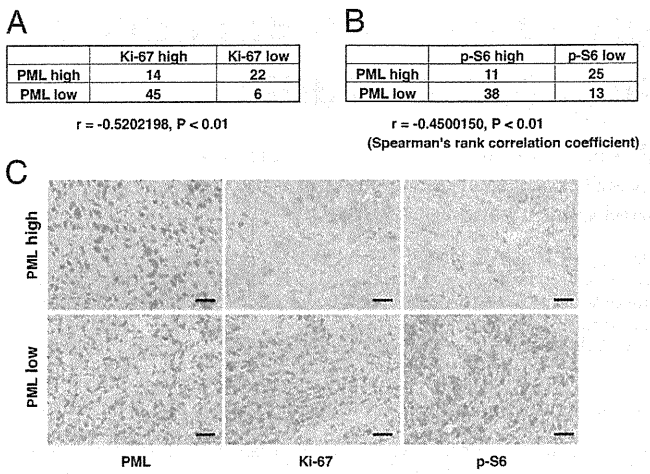

Fig. 1. PML is inversely correlated with proliferation rate and mTOR signaling in GBM clinical samples. (*A* and *B*) Tissue microarrays containing tumor samples from 87 GBM patients were stained by using PML, Ki-67, and p-S6 antibody, respectively. PML is highly expressed in 40% of GBM patients. Correlation analyses show PML significantly inversely correlate with Ki-67 (*A*) and p-S6 (*B*). (*C*) Immunohistochemical staining of (reddish brown) PML, Ki-67, and p-S6 from a representative GBM patient. (Magnification: 10×.) Nuclei were counterstained with hematoxylin (blue). (Scale bar: 100 μm.)

significantly inversely correlated with the cell proliferation marker Ki-67 (Fig. 1 *A* and *C*; $r = -0.52$, $P < 0.01$) and with mTORC1 signaling, as measured by S6 phosphorylation (Fig. 1 *B* and *C*; $r = -0.45$, $P < 0.01$).

Rapamycin Induces Expression and Nuclear Aggregation of PML. Next, we treated GBM cells and a GBM patient-derived cell culture with rapamycin to determine the effect of RTK/PI3K/mTOR inhibitor on PML (Fig. 2 *A–C*). Exposure to rapamycin treatment, or the ATP-competitive mTOR kinase inhibitor pp242, at doses sufficient to inhibit mTORC1 signaling, led to time-dependent increases in PML expression (Fig. 2 and Fig. S1). The EGFR tyrosine kinase inhibitor, erlotinib, which inhibited mTORC1 signaling downstream of EGFR, similarly elevated PML expression (Fig. 2*B*). Biochemical results were confirmed by fluorescent immunocytochemical analyses, demonstrating strongly granular patterns of PML staining in the nucleus, consistent with its reported distribution (Fig. 2*C*).

Overexpression of PML Contributes to Decreasing PI3K/Akt/mTOR Signaling and a Slower Cell Cycle. We hypothesized that PML might contribute to rapamycin, mTOR kinase inhibitor, and/or EGFR tyrosine kinase inhibitor resistance in GBM. Therefore, we performed retroviral transduction of PML I into U87 cells and examined the effect on PI3K/Akt/mTOR signaling and cell cycle progression. First, we performed double-immunofluorescent staining with PML and HA tag to confirm the overexpression of PML I (Fig. 3*A*). Compared with control, the retroviral-infected U87 cells expressed exogenous PML in both their nuclei and cytoplasm. Immunoblot analyses of these lysates demonstrated the increased expression of all PML isoforms, which would result from alternative splicing of the longest form, PML I (9). After confirmation of PML overexpression in these cell lines, we examined several PI3K/Akt/mTOR signaling proteins and cell cycle-related proteins by Western blotting. Akt and S6 phosphorylation were significantly decreased in U87 GBM cells that exogenously expressed PML I. Moreover, the cell cycle related proteins, cyclin D1 and cyclin-dependent kinase inhibitor 1 (p21), were also notably decreased, suggesting that PML contributes to decreasing PI3K/Akt/mTOR signaling and slowing down the cell cycle (Fig. 3*B*). We further performed cell proliferation assays by using these cell lines and confirmed that U87PML I cells were significantly less proliferative than control U87 cells (Fig. 3*C*; $^{**}P < 0.01$).

Flow cytometric cell cycle analyses demonstrated an increased G1 fraction in U87PML I-expressing GBM cells (Fig. 3*D*; $^{**}P < 0.01$). To determine whether this conferred rapamycin resistance, we treated U87PML I cells and control cells with rapamycin for 48 h and analyzed the drug effect by using WST-1 assays. PML I overexpression significantly reduced the growth inhibitory effect of rapamycin (Fig. 3*E*; $^{**}P < 0.01$).

Interfering RNA-Mediated PML Knockdown Sensitizes GBM Cell Lines to mTOR and EGFR Kinase Inhibitor Treatment. To confirm a specific role for PML in preventing mTOR and EGFR-kinase inhibitor-dependent cell death, we induced small interfering RNAs (siRNA)-mediated PML knockdown in multiple GBM cell lines and assessed its impact on response to rapamycin, pp242, and erlotinib. TUNEL analysis demonstrated that PML knockdown significantly sensitized all of the GBM cell lines to pp242 and erlotinib-mediated cell death (Fig. 4 *A* and *B*; $^{*}P < 0.05$, $^{**}P < 0.01$), which was confirmed by analysis of polyADP ribose polymerase (PARP) cleavage (Fig. S2). Of note, in contrast to pp242, rapamycin, which has less activity against mTORC2 than does pp242, induced minimal cell death even in the presence of PML knockdown, potentially suggesting a role for sustained mTORC2 signaling in mediating survival (7). Taken together, these data demonstrate that PML contributes to mTOR and EGFR kinase inhibitor resistance in GBM by suppressing tumor cell death, which can be reversed by pharmacological or genetic inhibition of PML.

As_2O_3 Abrogates pp242-Induced PML Up-Regulation and Sensitizes GBMs to mTOR Kinase Inhibitor-Mediated Cell Death. Arsenic trioxide (As_2O_3) has long been used as a therapeutic agent for promyelocytic leukemia (19–21). Besides its cell toxicity, As_2O_3 has been shown to target PML for degradation through a sumoylation-dependent process leading to PML polyubiquitination and proteosomal degradation (11, 13, 22–24). Therefore, we investigated the effect of As_2O_3 on reduction of PML in U87 cells. Single As_2O_3 treatments reduced PML expression at both low (0.15 μM) and high concentrations (2 μM) and decreased proliferation in serum-containing growth condition (Fig. S3 *A* and *B*). Notably, a high concentration (2 μM) induced an increase in p53 levels and decreased levels of cyclin D1 expression (Fig. S3*A*). The ability of low dose As_2O_3 to inhibit proliferation in the absence of p53 induction is consistent with previous papers (13, 25)

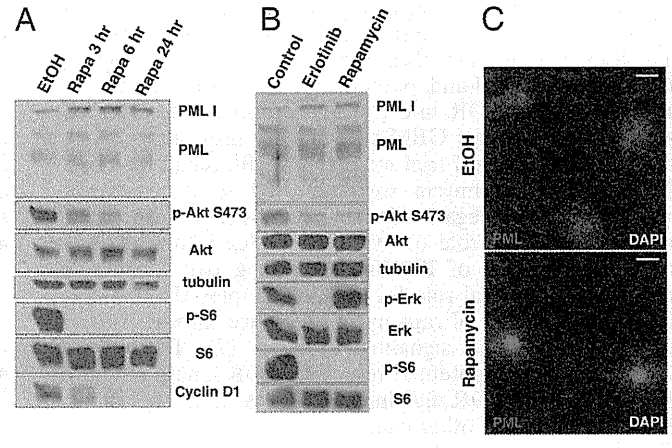

Fig. 2. PI3K/Akt/mTOR inhibitors induce PML expression in GBM cells. (*A*) Western blot analysis of the effect of rapamycin treatment on PML expression in U87 cells. Cells are cultured in serum-free condition. (*B*) Effect of the EGFR inhibitor erlotinib and rapamycin on PML expression in GBM patient-derived cells. Cells are cultured under neurosphere conditions. (*C*) Immunofluorescence of PML (red) in U87 cells treated with rapamycin or control. Nuclei are stained with DAPI (blue). (Scale bar: 20 μm.)

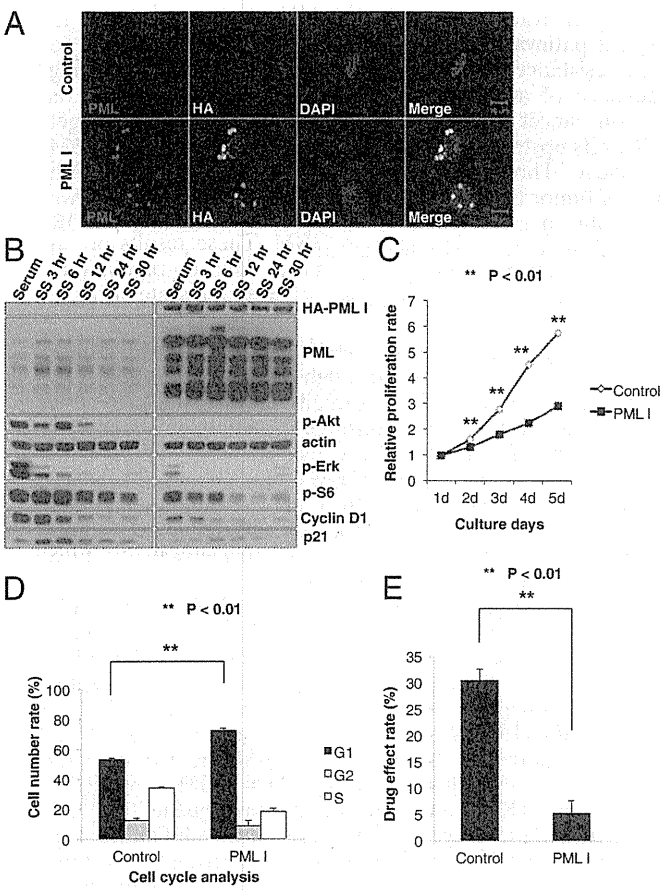

Fig. 3. PML overexpression decreases PI3K/Akt/mTOR signaling and slows down cell cycle. (*A*) Immunofluorescence in U87 control or hemagglutanin-tagged PML1 (HA-PMLI) infected cells. (Scale bar: 10 μm.) (*B*) Western blot analysis of PI3K/Akt/mTOR signaling pathway and cell cycle-related proteins performed on lysates from U87 control or HA-PMLI infected cells. Cells were placed in serum-free medium, cultured, and collected in each time course. (*C*) Proliferation of U87 control and HA-PMLI infected cells analyzed by WST assay. *P* value was determined by Student's *t* test. (*D*) Effect of PMLI overexpression on cell cycle progression in U87 cells. Cell cycle distribution was performed by flow cytometric analysis. *P* value was determined by Student's *t* test. (*E*) Effect of treatment with rapamycin on growth of U87 control and HA-PMLI infected cells analyzed by WST assay. *P* value was determined by Student's *t* test.

suggesting that lower concentration of As_2O_3 mediates its effect by reducing PML levels and not by inducing DNA damage. Neither pp242, nor As_2O_3 alone, promoted extensive tumor cell death. In contrast, As_2O_3 (0.15 μM) significantly and synergistically promoted pp242- dependent apoptotic cell death, as measured by cleaved caspase and TUNEL staining, independent of any effect on p53 phosphorylation (*$P < 0.01$; Fig. 5 *A* and *B* and Fig. S3*C*).

Therefore, we analyzed the effect of combining the mTOR kinase inhibitor pp242 with As_2O_3 on PML expression, cell death, and tumor size in U87 GBM xenografts (Fig. 5 *C*–*F*). Sixteen days of treatment with pp242 and As_2O_3, significantly reduced the growth of GBMs by nearly threefold ($P < 0.0005$) and induced TUNEL-positive cell death, an effect that was not detected with either pp242 or As_2O_3 monotherapy (Fig. 5 *C*, *D*, and *F*). Importantly, As_2O_3 also abrogated the pp242-mediated up-regulation of PML expression (Fig. 5*E*). Ki-67 staining was also diminished, although the decrease failed to reach statistical significance (Fig. S4). Taken together, these results demonstrate that As_2O_3 dramatically synergizes with mTOR kinase inhibition to promote GBM cell death and block tumor growth in vivo.

Immunohistochemical Analyses of PML Expression in GBM Patients Treated with Rapamycin or Erlotinib. Finally, to establish clinical relevance and to determine whether PML up-regulation is associated with mTOR and EGFR inhibitor resistance in GBM patients, we performed immunohistochemical analyses of tumor samples obtained from two "biopsy-treat-biopsy" paradigm phase I clinical trials, for which tumor tissue was obtained 7–10 d after treatment with rapamycin or lapatinib (details presented in refs. 6 and 26). As shown in Fig. 6, rapamycin (Fig. 6 *A* and *B*) and erlotinib (Fig. 6 *C* and *D*) treatment were both associated with significantly enhanced nuclear PML expression (*$P < 0.01$).

Discussion

PML is a pleiotropic tumor suppressor protein that is lost in many cancer types (12, 27). PML negatively regulates Akt-mTOR signaling (14, 28) and suppresses PTEN loss- induced prostate tumorigenesis (14) and mTOR-dependent renal carcinoma progression (28). We provide evidence from preclinical models and in patients that PML suppresses Akt/mTOR signaling and proliferation (Fig. 1). However, PML is also commonly overexpressed in cancer, including in GBM (12, 29), and has been shown to promote a range of activities that may enhance the growth and progression of cancer, including oncogene-induced senescence (29), hematopoetic stem cell maintenance, and breast cancer tumor cell survival through a peroxisome

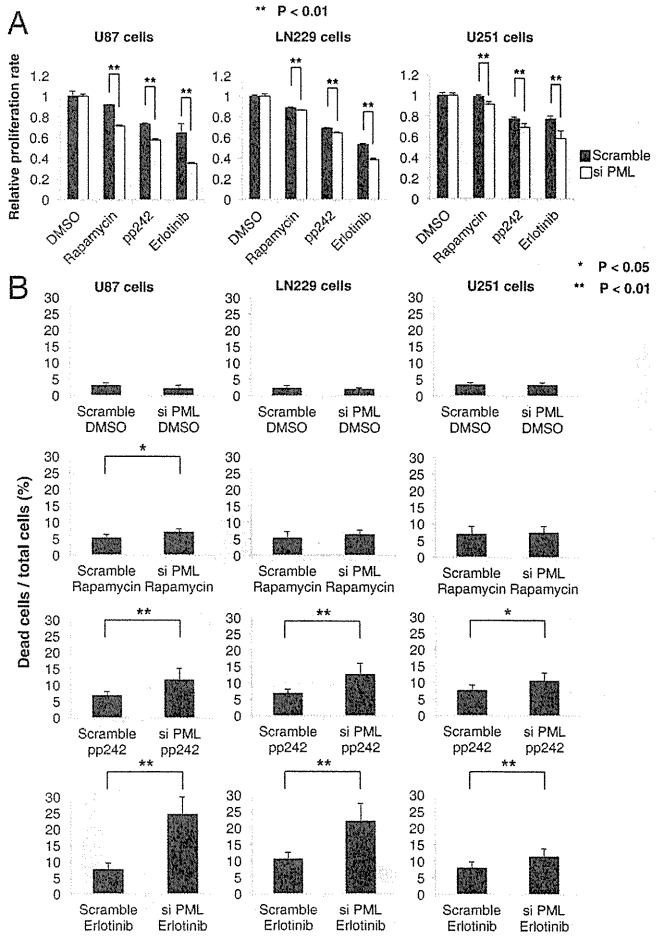

Fig. 4. PML knockdown sensitizes GBM cell lines to EGFR and mTOR targeted therapies. (*A*) Cell viability assays demonstrate a synergistic effect of PML knockdown and each indicated inhibitor. *P* values were determined by Student's *t* test. (*B*) Effect of PML knockdown and each indicated inhibitor on multiple GBM cell lines analyzed by Trypan blue exclusion. *P* values were determined by Student's *t* test.

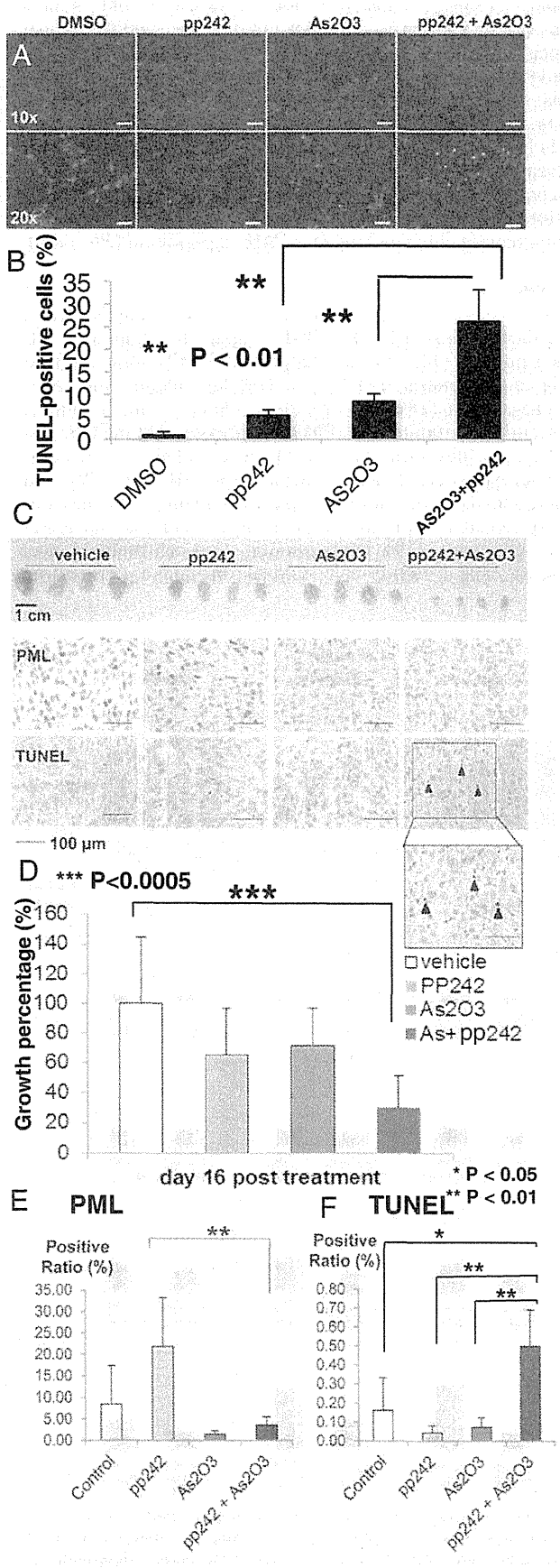

Fig. 5. As_2O_3 reduces PML and sensitizes GBM cells to mTOR-targeted therapies. (*A*) Representative images demonstrating TUNEL staining (green) to assess apoptotic effect of pp242 and As_2O_3 (2 μM) on U87 cells in vitro. Nuclei are stained blue. (*B*) Quantification of TUNEL staining. *P* values were determined by Student's *t* test. (*C*) Representative photographs of U87 GBM xenografts treated daily with vehicle, pp242 (60 mg/kg per day by oral gavage), As_2O_3 (2.5 mg/kg intraperitoneally), or combination ($n = 8$ mice per condition). Images of representative PML and TUNEL stains. (*D*) Quantification demonstrating greater than threefold reduction in tumor size for mice treated with combined pp242 and As_2O_3 ($P < 0.005$). (*E* and *F*) Quantification of PML and TUNEL xenograft tumor staining from each treatment conditions.

proliferator-activated receptor (PPAR)-γ/fatty acid oxidation-dependent pathway (30, 31). Further, PML has been shown to mediate resistance of leukemias to chemotherapy by supporting maintenance of a "quiescent" tumor cell population (13). Its impact on cancer drug resistance, including drugs that target mTOR or its upstream effectors, in solid tumors including GBM is less clear. Through integration of preclinical studies with analysis of tumor tissue from patients in phase I clinical trials, we demonstrate an important role for PML in mediating mTOR and EGFR inhibitor resistance in GBM. These results present evidence that mTOR inhibition promotes PML up-regulation in patients and that this up-regulation of PML mediates drug resistance.

It is tempting to speculate that PML promotes this resistance by inducing a "quiescent state" through inhibition of Akt/mTOR signaling. However, we cannot formally exclude the possibility that PML may drive resistance through its metabolic prosurvival effects. In fact, this possibility is consistent with our previous observation that EGFR mutant GBMs have enhanced reliance on fatty acid synthesis for survival (17), creating enhanced dependence on fatty acid oxidation for survival (32). Futures studies will be needed to determine the mechanisms by which PML promotes drug resistance in GBM.

mTOR has emerged as a critical target in GBM because it is persistently hyperactivated downstream of the most common GBM alterations including EGFR amplification, EGFR variant III (EGFRvIII) mutation, platelet-derived growth factor receptor (PDGFRα) and hepatocyte growth factor receptor (c-MET) amplification, and PTEN loss (3). We have demonstrated that mTOR inhibition is required for the efficacy of EGFR-targeted therapies (33), suggesting a mechanistic basis by which EGFR tyrosine kinase inhibitors (TKIs) may also potently up-regulate PML expression to promote drug resistance. For both EGFR TKIs and mTOR kinase inhibitors, the potential for converting a cytostatic response, which often yields minimal benefit, to a cytotoxic response by pharmacologically abrogating PML, could potentially represent a significant clinical advance. Our demonstration of a synergism between the two classes of compound in cell death induction underscores this possibility.

Pharmacologically targeting PML represents one of the most exciting success stories for the principle of molecularly guided therapies (10, 11). As_2O_3 targets PML for degradation through a SUMOylation-dependent process (34), potently promoting long-term remission in patients and mice with acute promyelocytic leukemia bearing the PML/RAR fusion (24). Its role in solid cancers has yet to be established. However, As_2O_3 given with standard chemotherapy can be tolerated by GBM patients, as demonstrated in recent clinical trials (35). The results presented here suggest a clinically actionable strategy to combine resistance by combining As_2O_3 with mTOR kinase and EGFR TKIs for the treatment of GBM patients.

Materials and Methods

Cell Lines. U87, LN229, and U251 GBM cell lines were cultured as previously described (18, 26). Brain tumor samples were collected after surgical resection under University of California, Los Angeles (UCLA) institutional review board-approved protocols between 1999 and 2011 from patients who gave informed consent, and graded by the neuropathologist in accordance with World Health Organization-established guidelines. Neurosphere cultures were prepared as described (36). Full details are provided in *SI Materials and Methods*.

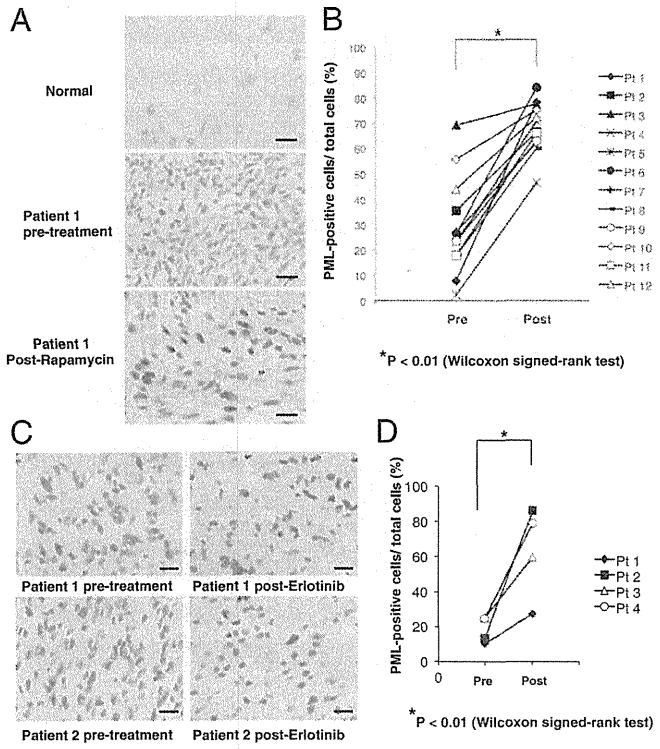

Fig. 6. Rapamycin and erlotinib treatment induces PML expression in GBM patient tumor tissues. (*A*) Immunohistochemical staining (reddish brown) of PML before and after treatment with rapamycin. Nuclei were counterstained with hematoxylin (blue). (*B*) Quantification of immunohistochemical staining from >1,000 cells from at least three representative areas of each tumor before and after rapamycin treatment. *P* value was determined by Wilcoxon signed-rank test. (*C*) Immunohistochemical staining (reddish brown) of PML before and after treatment with erlotinib. Nuclei were counterstained with hematoxylin (blue). (*D*) Quantification of immunohistochemical staining from >1,000 cells from at least three representative areas of each tumor before and after erlotinib treatment. *P* value was determined by Wilcoxon signed-rank test. (Scale bars: 50 μm.) (Magnification: 20×.)

Antibodies and Reagents. We used antibodies directed against the following: phosopho-Akt Ser473, Akt, phospho-S6 Ser235/236, S6, phospho-Erk, Erk, CyclinD1, cleaved PARP (Cell Signaling); β-actin, p21 (Sigma); phospho-EGFR Tyr1086 (Invitrogen); EGFR (Millipore); PML (for Western blotting, Abcam; for immunohistochemisry, Santa Cruz). Reagents used are rapamycin, As_2O_3, polybrene (Sigma), erlotinib (ChemieTex), pp242 (Chemdea). Full details of immunoblot analysis are provided in *SI Materials and Methods*. Stock solutions of inhibitor for rapamycin were made by dissolving in ethanol, erlotinib, and pp242 were made by dissolving in DMSO (Sigma) and stored at −20 °C. Inhibitors were added to each well at final concentrations of 10 nM, 10 μM, and 2 μM, respectively. An equal concentration of ethanol or DMSO served as control. As_2O_3 was diluted by PBS and 10 M NaOH, then pH was adjusted at 8.0 by 12 M HCl.

Plasmid, Retroviral Infection, and siRNA Transfection. Plasmid 22(pLNCX) encoding hemagglutinin (HA) tag-expression construct was obtained from the I.K. laboratory (37). Full details are available in *SI Materials and Methods*. Transfection of siRNA into GBM cell lines was carried out by using Lipofectamine RNAiMAX (Invitrogen) in full serum, with medium change after 24 h. On-TARGET plus SMARTpool siRNAs (Dharmacon) specifically targeting PML (catalog no. L-006547-000005) and nontargeting control pools of siRNAs (catalog no. D-0018-10-10-05) were used at 10 nM, and cells were harvested 48 h after transfection.

Cell Proliferation and Death Assays. Relative proliferation to control cells with vehicle treatment was checked with a WST-1 Cell Proliferation Assay Kit (Millipore). Cell death was assessed by Trypan blue exclusion (Invitrogen). Full details are given in *SI Materials and Methods*.

Cell Cycle Analyses. Cells were fixed in 70% ethanol diluted in PBS, and the samples were stored at −20 °C. The fixed cells were resuspended in PBS containing 20 μg/mL propidium iodide (Sigma) and 10 μg/mL RNase A (Sigma), and incubated for 10 min at 37 °C. Flow cytometric analysis was performed by using FACSCalibur flow cytometer (Becton Dickinson).

TUNEL Staining and Immunofluorescence Analysis. For TUNEL staining, cells were placed in eight-well chamber slides, incubated with TUNEL Reaction Mixture (Roche) at 37 °C for1 h in the dark, and visualized with a fluorescene microscope (Olympus BX-61). Ten separate, randomly chosen fields on each chamber were imaged, and the numbers of TUNEL-positive cells and whole nuclei were counted. For immunofluorescence analysis with indicated antibodies, cells were fixed with 4% paraformaldehyde in PBS for 10 min, washed twice in PBS, incubated with primary antibodies in PBS containing 3% BSA at 4 °C overnight, and detected with appropriate fluorescence-conjugated secondary antibodies. Full details are presented in *SI Materials and Methods*.

In Vivo Studies. We suspend 1.25×10^6 U87 GBM cells in 100 μL of Matrigel, PBS 1:2 solution, and injected them subcutaneously into the right flank of each 4- to 5-wk-old athymic nude mice. Tumors were measured with an electronic caliper, and volumes were calculated by using width (*a*), length (*b*), and depth (*c*) measurements ($V = a \times b \times c$). Ten days after injection, mice were treated daily with vehicle, 60 mg/kg pp242 by gavage, 2.5 mg/kg intraperitoneally injected As_2O_3 or their combination, respectively. Mice were euthanized when tumor volume of treated mice reached statistical significance compared with control groups. Mice were euthanized in accordance with the University of California at San Diego Institutional Guidelines for Animal Welfare and Experimental Conduct.

Immunohistochemical Assays, Tissue Microarrays, and Image Analysis-Based Scoring. Immunohistochemical staining and analysis of two GBM TMAs was performed, as described (6, 26). Among 140 cases, 87 GBM patient tissue cores were available for analysis based on sufficient high quality tissue. Staining intensity was scored independently by two pathologists who were unaware of the findings of the molecular analyses. See *SI Materials and Methods* for full details.

Statistical Analysis. Results are shown as mean ± SEM. χ^2 for independence test was used to assess correlations between various molecular markers on TMAs. For nonparametric clinical trial data, Wilcoxon rank test was used. Other comparisons in cell proliferation assays, cell death assays, and TUNEL staining were performed with Student's *t* test, as by analysis of variance, appropriate. $P < 0.05$ was considered as statistically significant.

ACKNOWLEDGMENTS. We thank Dr. George Thomas for helpful discussions and comments on this paper. A.I. and J.K. were supported in part by a grant from the Japan Society for the Promotion of Science. A.I. was also supported by a grant from the Uehara Memorial Foundation. B.G. is supported by a Marie Curie Fellowship from the European Commission- PIOF-GA-2010-271819. C.Z. is supported by an American-Italian Cancer Foundation post-doctoral research fellowship. This work was supported by National Institutes of Health (NIH) Grants NS73831 and CA119347 (to P.S.M.), by the Ziering Famiy Foundation in memory of Sigi Zeiring (P.S.M. and T.F.C.), the Ben and Catherine Ivy Foundation (P.S.M. and T.F.C.), and NIH Grant P01-CA95616 (to W.K.C.). W.K.C. is a Fellow of the National Foundation for Cancer Research.

1. Furnari FB, et al. (2007) Malignant astrocytic glioma: Genetics, biology, and paths to treatment. *Genes Dev* 21(21):2683–2710.
2. Wen PY, Kesari S (2008) Malignant gliomas in adults. *N Engl J Med* 359(5):492–507.
3. Anonymous; Cancer Genome Atlas Research Network (2008) Comprehensive genomic characterization defines human glioblastoma genes and core pathways. *Nature* 455(7216):1061–1068.
4. Parsons DW, et al. (2008) An integrated genomic analysis of human glioblastoma multiforme. *Science* 321(5897):1807–1812.
5. Yecies JL, Manning BD (2011) Transcriptional control of cellular metabolism by mTOR signaling. *Cancer Res* 71(8):2815–2820.
6. Cloughesy TF, et al. (2008) Antitumor activity of rapamycin in a Phase I trial for patients with recurrent PTEN-deficient glioblastoma. *PLoS Med* 5(1):e8.
7. Tanaka K, et al. (2011) Oncogenic EGFR signaling activates an mTORC2-NF-κB pathway that promotes chemotherapy resistance. *Cancer Discov* 1(6):524–538.
8. Bernardi R, Pandolfi PP (2003) Role of PML and the PML-nuclear body in the control of programmed cell death. *Oncogene* 22(56):9048–9057.
9. Bernardi R, Pandolfi PP (2007) Structure, dynamics and functions of promyelocytic leukaemia nuclear bodies. *Nat Rev Mol Cell Biol* 8(12):1006–1016.
10. Andre C, et al. (1996) The PML and PML/RARalpha domains: From autoimmunity to molecular oncology and from retinoic acid to arsenic. *Exp Cell Res* 229(2):253–260.

11. Chen GQ, et al. (1996) In vitro studies on cellular and molecular mechanisms of arsenic trioxide (As2O3) in the treatment of acute promyelocytic leukemia: As2O3 induces NB4 cell apoptosis with downregulation of Bcl-2 expression and modulation of PML-RAR alpha/PML proteins. *Blood* 88(3):1052–1061.
12. Gurrieri C, et al. (2004) Loss of the tumor suppressor PML in human cancers of multiple histologic origins. *J Natl Cancer Inst* 96(4):269–279.
13. Ito K, et al. (2008) PML targeting eradicates quiescent leukaemia-initiating cells. *Nature* 453(7198):1072–1078.
14. Trotman LC, et al. (2006) Identification of a tumour suppressor network opposing nuclear Akt function. *Nature* 441(7092):523–527.
15. Bernardi R, et al. (2004) PML regulates p53 stability by sequestering Mdm2 to the nucleolus. *Nat Cell Biol* 6(7):665–672.
16. Vallian S, et al. (1997) Transcriptional repression by the promyelocytic leukemia protein, PML. *Exp Cell Res* 237(2):371–382.
17. Guo D, et al. (2009) EGFR signaling through an Akt-SREBP-1-dependent, rapamycin-resistant pathway sensitizes glioblastomas to antilipogenic therapy. *Sci Signal* 2(101): ra82.
18. Lu KV, et al. (2009) Fyn and SRC are effectors of oncogenic epidermal growth factor receptor signaling in glioblastoma patients. *Cancer Res* 69(17):6889–6898.
19. Aronson SM (1994) Arsenic and old myths. *R I Med* 77(7):233–234.
20. Mathews V, et al. (2006) Single-agent arsenic trioxide in the treatment of newly diagnosed acute promyelocytic leukemia: Durable remissions with minimal toxicity. *Blood* 107(7):2627–2632.
21. Soignet SL, et al. (1998) Complete remission after treatment of acute promyelocytic leukemia with arsenic trioxide. *N Engl J Med* 339(19):1341–1348.
22. Lallemand-Breitenbach V, et al. (2001) Role of promyelocytic leukemia (PML) sumolation in nuclear body formation, 11S proteasome recruitment, and As2O3-induced PML or PML/retinoic acid receptor alpha degradation. *J Exp Med* 193(12):1361–1371.
23. de Thé H, Chen Z (2010) Acute promyelocytic leukaemia: Novel insights into the mechanisms of cure. *Nat Rev Cancer* 10(11):775–783.
24. Lallemand-Breitenbach V, Zhu J, Chen Z, de Thé H (2012) Curing APL through PML/RARA degradation by As2O3. *Trends Mol Med* 18(1):36–42.
25. Zhao S, Tsuchida T, Kawakami K, Shi C, Kawamoto K (2002) Effect of As2O3 on cell cycle progression and cyclins D1 and B1 expression in two glioblastoma cell lines differing in p53 status. *Int J Oncol* 21(1):49–55.
26. Mellinghoff IK, et al. (2005) Molecular determinants of the response of glioblastomas to EGFR kinase inhibitors. *N Engl J Med* 353(19):2012–2024.
27. Gambacorta M, et al. (1996) Heterogeneous nuclear expression of the promyelocytic leukemia (PML) protein in normal and neoplastic human tissues. *Am J Pathol* 149(6): 2023–2035.
28. Bernardi R, et al. (2011) Pml represses tumour progression through inhibition of mTOR. *EMBO Mol Med* 3(5):249–257.
29. Scaglioni PP, et al. (2012) Translation-dependent mechanisms lead to PML upregulation and mediate oncogenic K-RAS-induced cellular senescence. *EMBO Mol Med* 4(7):594–602.
30. Ito K, et al. (2012) A PML–PPAR-δ pathway for fatty acid oxidation regulates hematopoietic stem cell maintenance. *Nat Med* 18(9):1350–1358.
31. Carracedo A, et al. (2012) A metabolic prosurvival role for PML in breast cancer. *J Clin Invest* 122(9):3088–3100.
32. Cvrljevic AN, et al. (2011) Activation of Src induces mitochondrial localisation of de2-7EGFR (EGFRvIII) in glioma cells: Implications for glucose metabolism. *J Cell Sci* 124(Pt 17):2938–2950.
33. Wang MY, et al. (2006) Mammalian target of rapamycin inhibition promotes response to epidermal growth factor receptor kinase inhibitors in PTEN-deficient and PTEN-intact glioblastoma cells. *Cancer Res* 66(16):7864–7869.
34. Zhang XW, et al. (2010) Arsenic trioxide controls the fate of the PML-RARalpha oncoprotein by directly binding PML. *Science* 328(5975):240–243.
35. Grimm SA, et al. (2012) Phase I study of arsenic trioxide and temozolomide in combination with radiation therapy in patients with malignant gliomas. *J Neurooncol* 110(2):237–243.
36. Geschwind DH, et al. (2001) A genetic analysis of neural progenitor differentiation. *Neuron* 29(2):325–339.
37. Nguyen LA, et al. (2005) Physical and functional link of the leukemia-associated factors AML1 and PML. *Blood* 105(1):292–300.

Cell Cycle 12:10, 1473–1474; May 15, 2013; © 2013 Landes Bioscience

Arsenic reverses glioblastoma resistance to mTOR-targeted therapies

Akio Iwanami,[1] Timothy F. Cloughesy,[2] Webster K. Cavenee[3] and Paul S. Mischel[3,*]

[1]Department of Orthopaedic Surgery; Keio University School of Medicine; Tokyo, Japan; [2]Department of Neurology; David Geffen School of Medicine at UCLA; Los Angeles CA USA; [3]Ludwig Institute for Cancer Research; University of California at San Diego; La Jolla CA USA

The mammalian target of rapamycin, mTOR kinase is a compelling cancer drug target. mTOR, which exists in two distinct multi-protein complexes (mTORC1 and mTORC2), transduces growth factor receptor signals via the PI3K pathway and integrates them with nutrient and energy status to control a diverse array of functions including protein translation, glycolysis and lipogenesis.[1] Thus, mTOR serves as a critical regulatory node in the cell, controlling proliferation. In cancer, mutations in growth factor receptor signaling pathways persistently activate mTOR, supporting unrestrained tumor growth. The highly lethal form of adult brain cancer, glioblastoma (GBM), is one characteristic example. PI3K pathway activating mutations in growth factor receptor signaling pathways occur in nearly 90% of GBMs,[2] with frequent amplification and mutation of EGFR and deletion and mutation of PTEN,[2] providing compelling rationale for mTOR inhibitor therapy. However to date, attempts to target mTOR in GBM patients have failed. The allosteric mTOR inhibitor rapamycin and its analogs show no clinical benefit, failing to fully suppress mTORC1 signaling and paradoxically reactivating Akt signaling in tumor tissue[3] including through an mTORC2-dependent feedback loop.[4] ATP-competitive mTOR kinase inhibitors and dual PI3K/mTOR kinase inhibitors that can potentially suppress both mTORC1 and mTORC2 signaling have moved forward into early clinical testing in GBM. However, it is anticipated that other mechanisms of resistance may arise.

In a recent paper, we showed that the promyelocytic leukemia protein (PML), promotes a highly unexpected, but potentially targetable mechanism of mTOR inhibitor resistance in GBM.[5] PML is the core component of a nuclear substructure (PML nuclear bodies) that contains more than 70 proteins to enact a diverse array of functions including regulation of gene transcription and protein modification.[6] PML's relevance to cancer was first highlighted by its identification as part of the PML-RARα fusion oncogene in acute promyelocytic leukemia (APL). Remarkably, adding arsenic trioxide (ATO), which was derived from an ancient Chinese herbal formula and was subsequently shown to target PML for degradation through SUMOylation-dependent ubiquitination, induces complete remission or cure in this previously deadly form of cancer, providing one of the most compelling success stories for targeted cancer therapy and suggesting the potential targetability of PML in the clinic.[7] PML also appears to play an important role in other cancers. In chronic myeloid leukemia, PML initiates a quiescent state, enabling tumor to evade cytotoxic chemotherapy, which can be overcome by the addition of ATO.[8]

In solid cancers, the role of PML and its impact on treatment response is less certain. We hypothesized that PML could render GBMs resistant to mTOR targeted therapies by inducing quiescence through suppression of mTOR signaling. Immunohistochemical analysis of GBM clinical samples demonstrated that PML expression was inversely correlated with mTOR signaling and with Ki67 labeling, a measure of tumor cell proliferation. Mechanistically confirming these observations, overexpression of PML suppressed mTOR signaling and limited proliferation in GBM cells. Further, in glioblastoma cell lines, xenograft models and most importantly in tumor tissue from patients treated with rapamycin or erlotinib, mTOR inhibition resulted in potent upregulation of PML levels. Genetic depletion of PML by siRNA knockdown, or treatment with low dose ATO sensitized GBM cells mTOR inhibitor-mediated tumor cell death, converting the normal cytostatic response to an apoptotic one. Most importantly, in tumor xenografts, ATO and the mTOR kinase inhibitor pp242 were relatively ineffective when given alone, but potently synergized, suppressing PML upregulation and causing massive tumor cell death.[5]

These results raise a number of intriguing questions. mTOR is a compelling drug target in multiple solid cancer types. Does PML upregulation similarly contribute to mTOR inhibitor resistance in other cancer types, and if so, is it similarly targetable by ATO? mTOR and PML are both critical regulatory nodes in the cell, each functioning as a rheostat to "tune" and integrate complex signaling cascades. What are the mechanisms by which PML becomes upregulated in response to mTOR inhibition and do they present a potential drug targets? PML is considered to be a tumor suppressor, but its role in promoting cancer drug resistance, demonstrates a more nuanced function, hindering or aiding tumor survival depending on genetic and biochemical context. Well-designed clinical trials combining mTOR inhibitors with ATO may improve the outcome for GBM patients and are likely to shed new light on the role of PML in cancer, particularly with regard to its interaction with mTOR. (**Fig. 1**)

*Correspondence to: Paul S. Mischel; Email: pmischel@ucsd.edu
Submitted: 04/08/13; Accepted: 04/13/13
http://dx.doi.org/10.4161/cc.24747

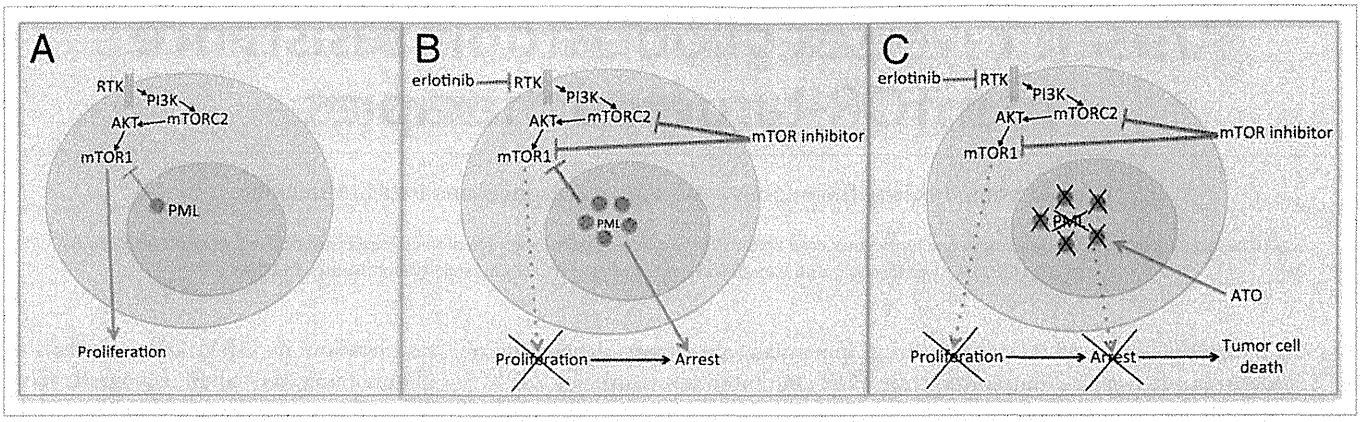

Figure 1. PML mediates resistance to mTOR targeted therapies in GBM, which is reversed by ATO. (**A**) Schematic diagram showing that persistent mTOR signaling promotes tumor cell proliferation, while PML opposes it. (**B**) In GBMs treated with mTOR inhibitors or EGFR inhibitors such as erlotinib that also block mTOR signaling, PML is upregulated, promoting tumor cell arrest. (**C**) ATO, which leads to degradation of PML protein, synergizes with mTOR inhibitors, potently causing tumor cell death.

References

1. Laplante M, et al. Cell 2012; 149:274-93; PMID:22500797; http://dx.doi.org/10.1016/j.cell.2012.03.017
2. Cancer Genome Atlas Research Network. Nature 2008; 455:1061-8; PMID:18772890; http://dx.doi.org/10.1038/nature07385
3. Cloughesy TF, et al. PLoS Med 2008; 5:e8; PMID:18215105; http://dx.doi.org/10.1371/journal.pmed.0050008
4. Tanaka K, et al. Cancer Discov 2011; 1:524-38; PMID:22145100; http://dx.doi.org/10.1158/2159-8290.CD-11-0124
5. Iwanami A, et al. Proc Natl Acad Sci USA 2013; 110:4339-44; PMID:23440206; http://dx.doi.org/10.1073/pnas.1217602110
6. Carracedo A, et al. Curr Opin Cell Biol 2011; 23:360-6; PMID:21501958; http://dx.doi.org/10.1016/j.ceb.2011.03.011
7. Hu J, Liu YF, et al. Proc Natl Acad Sci USA 2009; 106:3342-7; PMID:19225113; http://dx.doi.org/10.1073/pnas.0813280106
8. Ito K, et al. Nature 2008; 453:1072-8; PMID:18469801; http://dx.doi.org/10.1038/nature07016
8. Matsuoka S, et al. Science 2007; 316:1160-6; PMID:17525332; http://dx.doi.org/10.1126/science.1140321

Zhou et al. Molecular Brain 2014, 7:24
http://www.molecularbrain.com/content/7/1/24

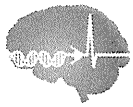

Molecular Brain

RESEARCH Open Access

Reprogramming non-human primate somatic cells into functional neuronal cells by defined factors

Zhi Zhou[1], Kazuhisa Kohda[1], Keiji Ibata[1], Jun Kohyama[1], Wado Akamatsu[1], Michisuke Yuzaki[1], Hirotaka James Okano[2], Erika Sasaki[1,3] and Hideyuki Okano[1*]

Abstract

Background: The common marmoset (*Callithrix jacchus*) is a New World primate sharing many similarities with humans. Recently developed technology for generating transgenic marmosets has opened new avenues for faithful recapitulation of human diseases, which could not be achieved in rodent models. However, the longer lifespan of common marmosets compared with rodents may result in an extended period for *in vivo* analysis of common marmoset disease models. Therefore, establishing rapid and efficient techniques for obtaining neuronal cells from transgenic individuals that enable *in vitro* analysis of molecular mechanisms underlying diseases are required. Recently, several groups have reported on methods, termed direct reprogramming, to generate neuronal cells by defined factors from somatic cells of various kinds of species, including mouse and human. The aim of the present study was to determine whether direct reprogramming technology was applicable to common marmosets.

Results: Common marmoset induced neuronal (cjiN) cells with neuronal morphology were generated from common marmoset embryonic skin fibroblasts (cjF) by overexpressing the neuronal transcription factors: *ASCL1*, *BRN2*, *MYT1L* and *NEUROD1*. Reverse transcription-polymerase chain reaction of cjiN cells showed upregulation of neuronal genes highly related to neuronal differentiation and function. The presence of neuronal marker proteins was also confirmed by immunocytochemistry. Electrical field stimulation to cjiN cells increased the intracellular calcium level, which was reversibly blocked by the voltage-gated sodium channel blocker, tetrodotoxin, indicating that these cells were functional. The neuronal function of these cells was further confirmed by electrophysiological analyses showing that action potentials could be elicited by membrane depolarization in current-clamp mode while both fast-activating and inactivating sodium currents and outward currents were observed in voltage-clamp mode. The 5-bromodeoxyuridine (BrdU) incorporation assay showed that cjiN cells were directly converted from cjFs without passing a proliferative state.

Conclusions: Functional common marmoset neuronal cells can be obtained directly from embryonic fibroblasts by overexpressing four neuronal transcription factors under *in vitro* conditions. Overall, direct conversion technology on marmoset somatic cells provides the opportunity to analyze and screen phenotypes of genetically-modified common marmosets.

Keywords: Common marmoset, Direct reprogramming, Induced neuronal cells, Transcription factor, Regenerative medicine, Disease modeling, Cell-fate plasticity, Transdifferentiation

* Correspondence: hidokano@a2.keio.jp
[1]Department of Physiology, Keio University School of Medicine, 35 Shinanomachi, Shinjuku-ku, Tokyo 160-8582, Japan
Full list of author information is available at the end of the article

Background

The common marmoset (*Callithrix jacchus*) is a New World primate that has recently attracted considerable attention as a non-human primate model for biomedical research [1]. Specific features of the common marmoset are its small size, ease of handling, high fertility, early sexual maturity, its similarity of physiological properties with humans, drug metabolism, and neurophysiological functions [1]. Thus far, transgenic mice modeling human neurodegenerative diseases have contributed to disease research and drug development. However, none of them have succeeded in faithfully recapitulating the full spectrum of disease pathologies observed in humans [2,3]. In a recent report by our group, transgenic marmosets with germline transmission were successfully generated for the first time by lentiviral vector-mediated gene transfer [4]. For these reasons, our novel transgenic non-human primate models may be suitable for studying human diseases, particularly those that are neurodegenerative, such as Alzheimer's and Parkinson's disease. These *in vivo* models are expected to faithfully recapitulate pathophysiology of human diseases, and thus provide for the missing link between mouse and human disease research with subsequent drug development. However, results of studies from these models may require an extended period because of the longer lifespan of common marmosets compared with mice [5]. Moreover, detailed *in vitro* analyses using primary neuronal cultures of the affected area of the common marmoset transgenic models are not realistic.

Recent studies using human neuronal cells derived from either pluripotent stem cells or somatic cells have succeeded in modeling human neurological disorders *in vitro* [6,7]. These results prompted us to develop a convenient and rapid method for obtaining common marmoset neuronal cells from accessible somatic cells. Therefore, we focused on somatic cell reprogramming technology, including induced pluripotent stem (iPS) cell and direct conversion technology [8,9]. However, few studies have succeeded in generating common marmoset iPS cells from neonatal skin fibroblasts, fetal liver cells, and adult bone marrow-derived cells [10-12]. Moreover, only a few protocols exist for obtaining functional common marmoset neuronal cells from pluripotent stem cells [13]. Furthermore, little attention has been given to the direct conversion technology of common marmoset dermal fibroblasts into neuronal cells thus far. Therefore, in the present study, we aimed to generate common marmoset neuronal cells directly from dermal fibroblasts. Our results provide the first line of evidence for the generation of electrophysiologically functional neuronal cells from common marmoset somatic cells by defined neuronal transcription factors.

Results and discussion

Validation of the lentivirus-mediated overexpression of neuronal transcription factors

Recently, generation of induced neuronal (iN) cells was reported using mouse and human dermal cells [9,14]. In the present study, we used a set of neuronal transcription factors for human iN cells on common marmoset embryonic skin fibroblasts (cjF) isolated from embryonic day 91 (E91) embryos to determine whether common marmoset somatic cells could be converted into neuronal cells. We first confirmed transgene expression in the mouse fibroblast cell line, NIH3T3, by infecting these cells with lentiviral vectors coding the neuronal transcription factors: *ASCL1*, *BRN2*, *MYT1L*, and *NEUROD1* [14], under the control of tetracycline response element (TRE) together with reverse tetracycline transactivator (rtTA)-expressing vector. Upregulation of transgenes in NIH3T3 cells after doxycycline (dox) treatment was confirmed by immunocytochemistry (Additional file 1).

Generation of neuron-like cells from common marmoset somatic cells

To address whether cjFs, which were immunonegative for the neural progenitor marker, SRY (sex determining region Y)-box 2 (Sox2) (data not shown), can be converted into cjiN cells, cjFs were infected with these lentiviral vectors at 0 day *in vitro* (div) (Figure 1A). Synapsin reporter-positive mouse iN cells have been shown to be more functionally mature than negative cells [15]. Therefore, the reporter lentivirus, which expresses fluorescent protein (enhanced green fluorescent protein or DsRed) under the control of the human synapsin I promoter, was used in the present study to monitor neuronal conversion of cjFs [16-18] (Figure 1A). When cjFs were treated with dox at 1 div to induce neuronal conversion (Figure 1B), synapsin reporter-positive cells with typical neuronal morphologies were observed (Figure 2A, B). However, cjFs without dox treatment did not generate synapsin reporter-positive cells (Figure 2A). Notably, the morphology of synapsin reporter-positive cells resembled fibroblasts at 9 div and then changed into neuronal ones during reprogramming (Figure 2A, B). The reprogramming efficiency was monitored by the number of synapsin reporter-positive cells with neuronal morphology, and depended on the concentration of dox yielding 0.3 ± 0.1, 21.8 ± 0.8, or 32.6 ± 2.6 cjiN cells/cm^2 at 16 div when treated with 0, 1, or 2 μg/mL dox, respectively (Figure 2C) ($P^{**} < 0.001$, $P^{\#\#} < 0.01$, n = 4). However, the overall induction efficiency was much lower (<1%) than those in previous studies using mouse and human fibroblasts [9,14]. This discrepancy was probably due to the low infection efficiency of lentivirus in cjFs compared with those in mouse and human fibroblasts. Previous studies have also shown that polycistronic vector, micro RNAs and small molecules can facilitate iN cell induction

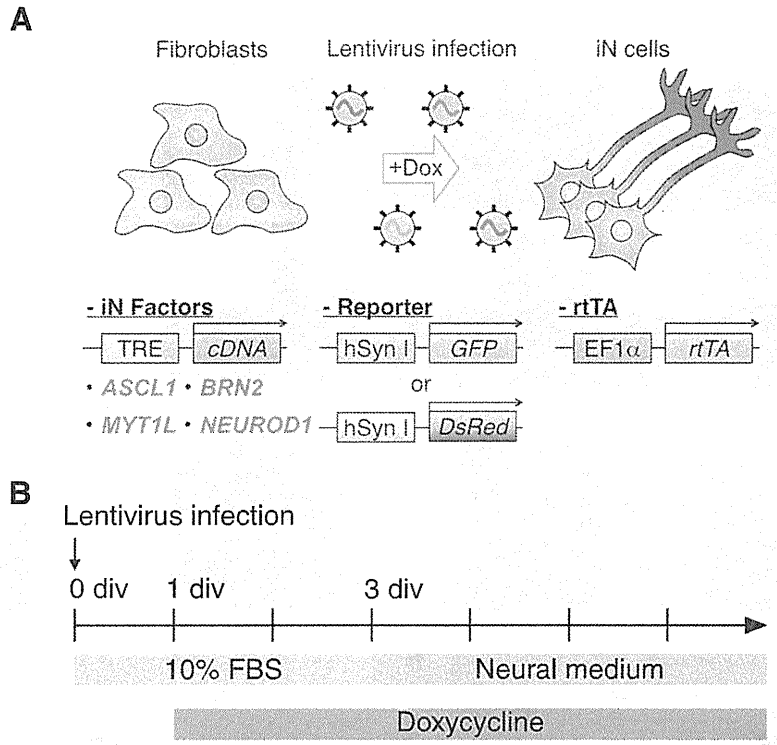

Figure 1 Schematic overview of the experimental procedure for generation of common marmoset induced neuronal cells from common marmoset embryonic skin fibroblasts. **(A)** Common marmoset embryonic skin fibroblasts (cjFs) were infected with drug-inducible lentiviral vectors coding a set of induced neuronal (iN) cell factors: *ASCL1*, *BRN2*, *MYT1L*, and *NEUROD1*. Synapsin reporter lentivirus expressing green fluorescent protein (GFP) or DsRed under the human synapsin I promoter was used to monitor neuronal induction. The lentiviral vector that stably drives *rtTA* expression under the EF1α promoter was transduced to induce the expression of iN-factors. **(B)** Time course for common marmoset induced neuronal (cjiN) cell induction. Lentivirus infection was conducted at 0 day *in vitro* (div) in fibroblast medium containing 10% fetal bovine serum, and cells were exposed to doxycycline (dox) at 1 div for cjiN induction. The culture medium was then replaced at 3 div with dox-containing neural meium composed of N2B27 medium, neurotrophin-3 (NT-3) and brain-derived neurotrophic factor (BDNF). For calcium imaging, the cAMP analog, 8-(4-Chlorophenylthio) adenosine 3′, 5′-cyclic monophosphate (8-CPT; 100 μM) [29], was added to promote neuronal maturation and survival.

[7,19,20]. Therefore, the induction conditions of cjiN cells may be optimized in the future study to enhance the conversion efficiency. Nevertheless, our results show that the four-factor set of neuronal transcription factors is sufficient to convert cjFs to cjiN cells.

The duration of dox treatment was critical for neuronal conversion

Next, we investigated the required duration of exogenous neuronal transcription factor expression to drive neuronal transdifferentiation. Therefore, we examined the exposure time of dox and the cjiN induction efficiency (Figure 2D). Treatment with dox from 1–3 div promoted the conversion of cjFs into synapsin reporter-positive cells with neuronal morphology (Figure 2E). Similarly, a previous study has shown that the endogenous neuronal transcriptional factor network is activated 48 h after dox treatment [14]. Our findings also revealed that the induction efficiency at 23 div depended on the exposure time of dox (Figure 2F). The treatment of cjFs with dox from 1–11 div followed by a culture without dox treatment from 11–23 div generated 112.1 ± 28.1 cjiN cells/cm^2 (Figure 2F). However, cells cultured with dox from 1–3 div followed by a culture without dox treatment from 3–23 div generated only 10.6 ± 5.4 cjiN cells/cm^2 (Figure 2F). The efficiency of the former group was significantly ($P^{***} < 0.001$, n = 4) higher (more than 10-fold) compared with the latter group (Figure 2F). These results indicate that a longer expression of exogenous neuronal transcriptional factors is required for efficient lineage conversion of somatic cells.

cjiN cells expressed a subset of neuronal genes and proteins

To characterize cjiN cells as neuronal cells, we performed reverse transcription-polymerase chain reaction (RT-PCR) analysis using bulk RNA samples, including the remaining synapsin reporter-negative cells to explore the expression of neuronal genes (see Table 1 for the primer sets used). We detected an upregulation of neuronal genes (Figure 3), which included cytoskeletal markers

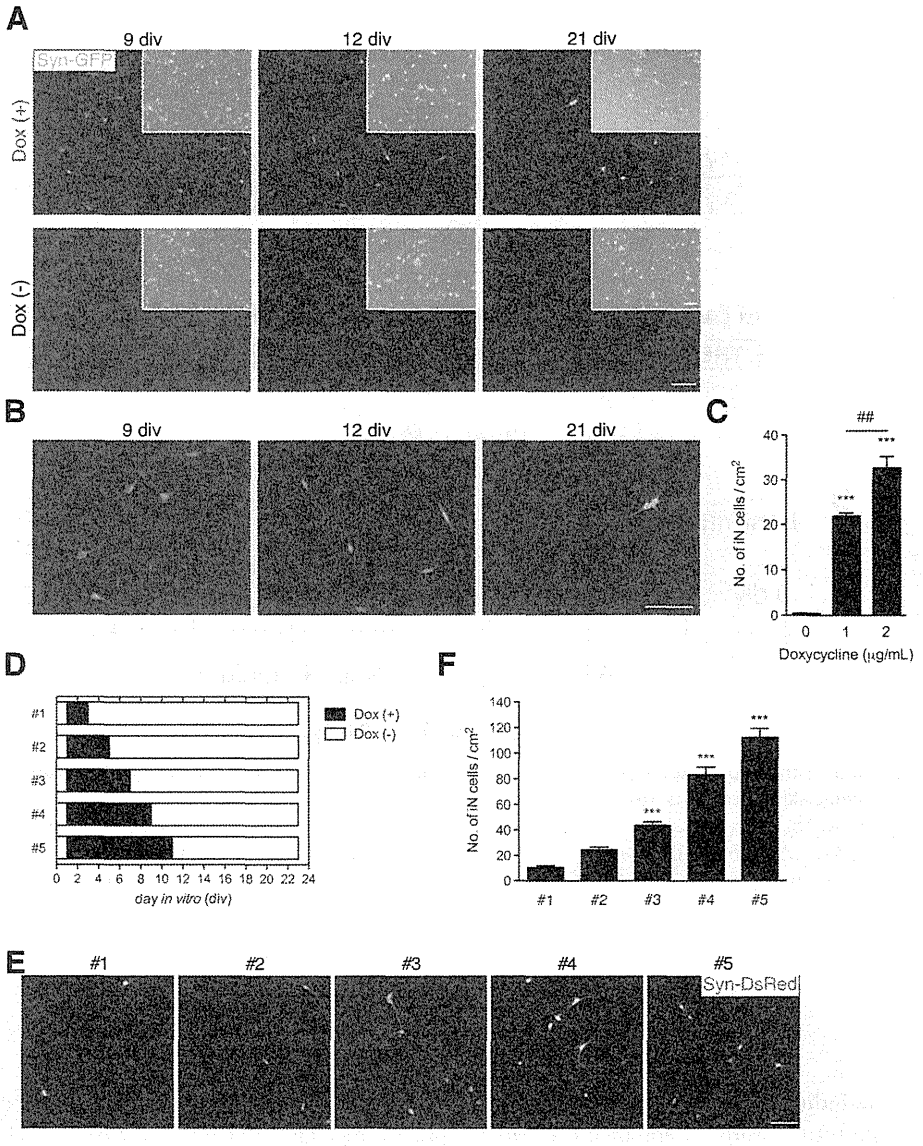

Figure 2 Generation of iN cells. (A, B) Transgene-dependent conversion of common marmoset fibroblasts into neuronal cells, in which synapsin reporter activation and morphological changes were dependent on the exogenous transcription factor and time. Cells became synapsin reporter-positive accompanied by a gradual morphological changes into neuronal cells, both effects of which were not found in cells cultured in neural medium without dox at 21 div. **(B)** Magnified images of Figure 1A showing synapsin reporter-positive cells with morphological changes from fibroblasts to neuronal cells. **(C)** Counts of synapsin reporter-positive cells with neuronal morphology showed a dox-dependent increase in their number (positive cells with fibroblast morphology were excluded from the counts). $P^{***} < 0.001$, $P^{\#\#} < 0.01$ (one-way ANOVA followed by Tukey's test). **(D-F)** The effect of sustained dox treatment on the production of cjiN cells. **(D)** Cells were treated with dox at 1 div until 3, 5, 7, 9 or 11 div and then maintained without dox until 23 div. **(E)** Synapsin reporter-positive cells with neuronal morphology were observed in all treatment group. **(F)** Cell counts revealed that a longer treatment time of dox increased the number of cjiN cells. Although dox treatment from 1–3 div sufficiently promoted cjiNs, a longer treatment time increased their number. $P^{***} < 0.001$ (one-way ANOVA followed by Tukey's test). Scale bar; 200 μm.

(*MAP2*, *DCX* and *TUBB3*), synaptic vesicle markers (*SYN1* and *VGLUT1*), and cation channel-related genes (*SCN1A*, *GRIN1* and *GRIA1*) in cjiN cells at 21 div (Figure 3). However, expression of these neuronal genes was not detected in cjFs at 0 div (Figure 3). These results were in line with the concentration-dependent induction efficiency of dox in Figure 2C. We also detected endogenous expression of *BRN2* and *NEUROD1* in cjiN cells at 21 div (Figure 3), indicating that ectopic expression of neuronal transcription factors activated the endogenous neuronal program. This effect may have caused neuronal transdifferentiation from somatic cells [9,14,21]. Thus, ectopic neuronal differentiation

Table 1 Primer sets used in RT-PCR analysis

Gene name	Forward primer	Reverse primer	Product size (bp)
SYN1	acggagactaccgcagtttg	cgatctgctccagcattgca	459
DCX	ctgtgcgtgtgcttctgaac	tcagctggagacttgcttcg	346
TUBB3	catagaccccagtggcaactacg	caccctccgtgtagtggcccttgg	241
MAP2	cctgtgttaagcggaaaacc	agagactttgtcctttgcctgt	86
VGLUT1	tcaataacagcacgacccac	tcccggaatttgagtgacaatg	131
SCN1A	attggcaattccgtgggagc	cccacacagcacgcggaaca	204
GRIN1	accccaagatcgtcaacatcg	ggctaaccagaatggcgtaga	213
GRIA1	cgagctttcctgttgatacat	tctgccacttgtaatggtcgatg	99
endo BRN2	aattaaggaaaaaggaaagcaact	caaaacatcattacacctgct	71
endo NEUROD1	gttattgtgttgccttagcacttc	agtgaaatgaattgctcaaattgt	77
ACTB	ggcatccacgaaactacctttt	acactgagtacttgcgctcg	202

signals are likely to work together with the endogenous neuronal program to efficiently convert non-neuronal cells into neuronal cells [21].

To further characterize the property of cjiN cells, we performed immunocytochemistry for the neuronal markers. The results showed that most synapsin reporter-positive cells also expressed (>88%) the pan-neuronal marker, microtubule-associated protein 2 (MAP2) (data not shown). This result indicated that the synapsin reporter using the sequence of human synapsin I promoter was also functional in common marmoset cells, and was thus a reliable reporter for neuronal conversion, as previously reported [15,16]. In cjiN cells at 43 div, MAP2-negative cells were found to be negative for glial fibrillary acidic protein and only weakly positive for α-smooth muscle actin (data not shown), raising the possibility that they were partially reprogrammed cells. The MAP2- and synapsin reporter-positive cells also showed immunoreactivity for the synaptic vesicle marker, synaptophysin, at 38 div (Figure 4A). However, immunostaining for synaptophysin and PSD95 revealed that these cells were unlikely to make synapse structures at 38 div (data not shown). Although the cjiN cells expressed neuronal marker genes and proteins, they did not appear to be mature enough to make synaptic contacts themselves. However, a future study may facilitate synaptic formation by improving induction efficiency and by co-culturing with astrocytes [9,14].

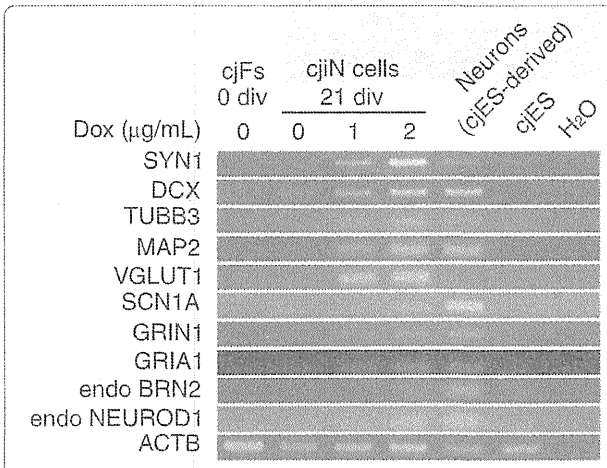

Figure 3 Neuronal marker gene expression in cjiN cells. Dox treatment upregulated cytoskeletal (*MAP2*, *DCX*, and *TUBB3*) and synaptic vesicular (*SYN1* and *VGLUT1*) marker genes, and cation channel-related genes (*SCN1A*, *GRIN1* and *GRIA1*). The results also showed the activation of endogenous *BRN2* and *NEUROD1* genes.

The majority of cjiN cells were glutamatergic

To characterize the neurotransmitter phenotype of iN cells, we examined the expression of neurotransmitters in MAP2-positive cjiN cells. Immunostaining at 38 div for vesicular glutamate transporter 1 (vGlut1) and gamma aminobutyric acid (GABA) revealed the presence of both excitatory glutamatergic and inhibitory GABAergic neuronal cells, respectively (Figure 4B). Counts of vGlut1 and GABA-positive cjiN cells showed a significantly ($P^{***} < 0.001$, n = 4) greater number of vGlut1-positive cells (39.2 ± 1.9/cm^2) than GABA-positive cells (16.4 ± 2.8 cells/cm^2) (Figure 4C). These results are in accordance with previous studies showing that the majority of iN cells are excitatory cells [7,14,22]. Our findings thus indicate that iN induction may be feasible in the future for the *in vitro* analysis of the transgenic common marmoset model of Alzheimer's disease, in which forebrain excitatory neurons are expected to be affected. Moreover, our cjiN cell induction protocol is likely advantageous over the previously reported neuronal differentiation protocol which used common marmoset embryonic stem (ES) cells and iPS cells, because the ES/iPS cell-derived neural precursor cells showed caudal identity [13]. Thus far, several groups have succeeded in generating reprogrammed neuronal cells with specific neuronal subtypes, such as dopaminergic neurons and motor neurons [23-26], which implicate the cell fate plasticity of terminally differentiated somatic cells.

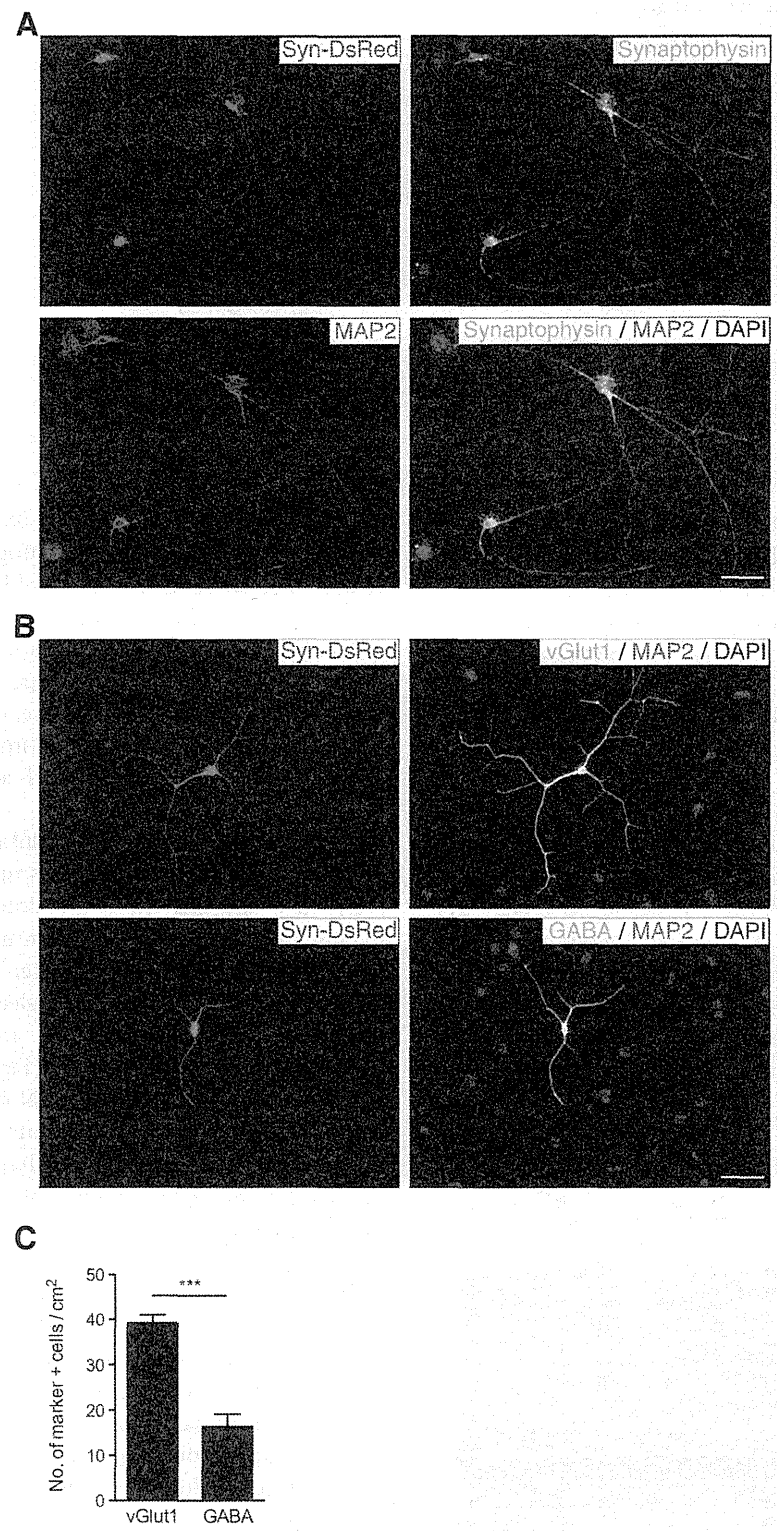

Figure 4 Immunocytochemistry of cjiN cells. (A) Synapsin reporter-positive-cjiN cells expressed microtubule-associated protein 2 (MAP2) and synaptophysin. **(B)** cjiN cells were vesicular glutamate transporter 1 (vGlut1)- and gamma-aminobutyric acid (GABA)-positive, thereby displaying a heterogeneous pool of excitatory and inhibitory neurons, respectively. **(C)** A significantly greater number of vGlut1-positive cells was generated compared with GABA-positive cells. $P^{***} < 0.001$ (Student's *t*-test). Scale bar; 50 μm.

Our success in reprogramming common marmoset somatic cells into excitatory and inhibitory neuronal cells using defined iN factors may therefore provide great promise in the future for generating specific subtypes of neuronal cells with specific sets of neuronal transcription factors.

cjiN cells were functional as matured neurons

To further confirm the successful conversion of cjFs into functional neuronal cells, we performed calcium imaging analysis. cjiN cells cultured with dox were incubated with the calcium indicator, Fluo-4 AM [13], followed by response recordings. The intracellular calcium level ($[Ca^{2+}]_i$) in cjiN cells at 15 div was increased in cjiN cells perfused with 80 mM of KCl, which was then decreased by washout (Additional file 2). Furthermore, electrical field stimulation on cjiN cells at 28 div increased $[Ca^{2+}]_i$, which was reversibly blocked by the voltage-gated sodium channel blocker, tetrodotoxin (0.2 μM) (Figure 5), suggesting that the increase in $[Ca^{2+}]_i$ was likely evoked by action potentials through voltage-gated sodium channels. These results showed that cjiN cells derived from cjFs were functionally comparable to common marmoset ES cell-derived neuronal cells [13], and thus strongly suggest that reprogramming of common marmoset somatic cells generates functional neuronal cells. Moreover, electrophysiological analyses of cjiN cells at 29–42 div revealed that action potentials were elicited by membrane depolarization in current-clamp mode in 17 out of 21 cjiN cells (81.0%) (Figure 6A and Additional file 3). Among these 17 cjiN cells, 7 cjiN cells (41.2%) generated a single action potential and the remaining 10 cjiN cells (58.8%) generated repetitive action potentials (Figure 6A and Additional file 3). In the voltage-clamp mode, both fast-activating and inactivating sodium currents and outward currents were observed (Figure 6B). The resting membrane potentials of cjiN cells ranged between -26 and -55 mV, with a mean ± SEM of -38.1 ± 2.0 mV (Figure 6C and Additional file 3). This mean value was significantly ($P^{***} < 0.001$) lower than that of cjFs (-16.4 ± 0.6 mV) with a range between -13.1 and -19.0 mV (Figure 6C and Additional file 3). Overall, our patch clamp recordings showed that cjiN cells are functional neuronal cells.

cjiN cells were directly converted from cjFs without passing through a proliferative state

To determine whether cjiN cells were directly converted from cjFs without passing through a proliferative neural

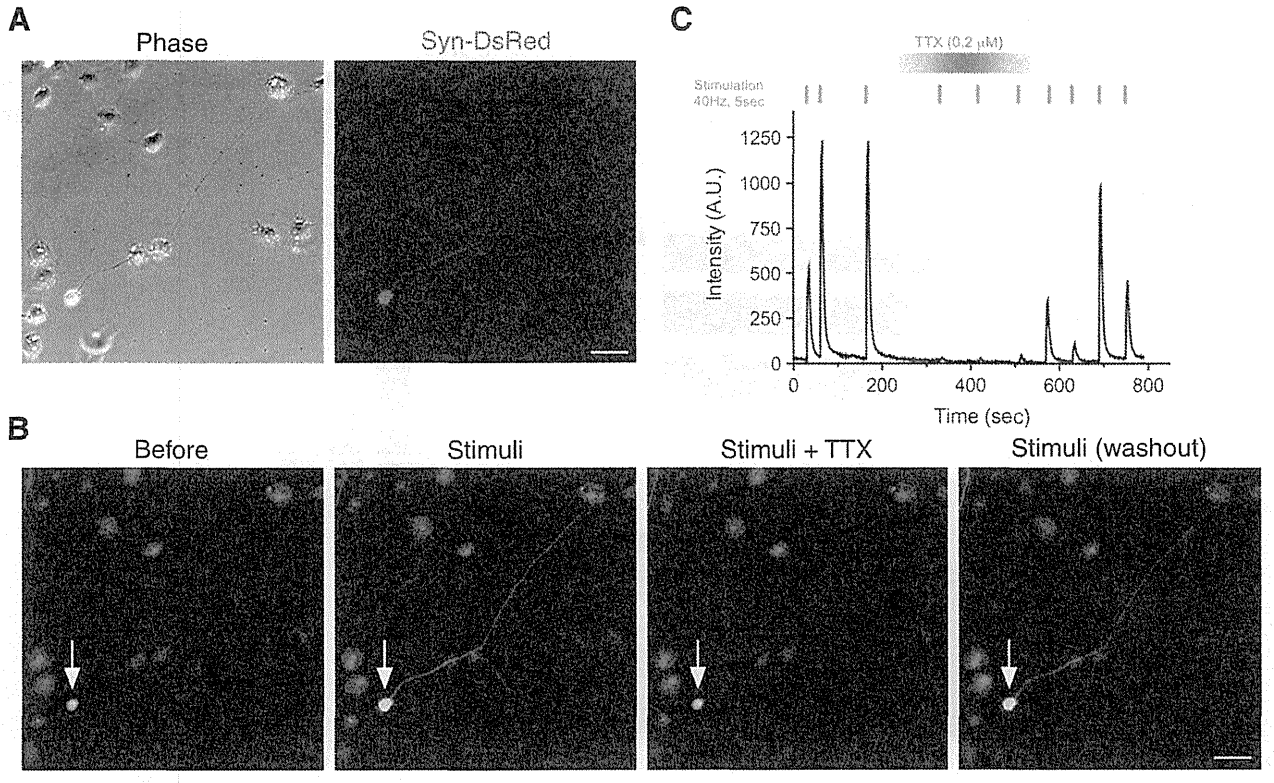

Figure 5 Increase in the intracellular calcium level upon electrical field stimulation. (A) cjiN cells (synapsin reporter-positive with a neuronal morphology). **(B, C)** Intracellular calcium level ($[Ca^{2+}]_i$) in cjiN cells was measured by the intensity of Fluo-4 fluorescence. Electrical field stimulation (40 Hz for 5 seconds) induces a robust elevation of $[Ca^{2+}]_i$ in some synapsin reporter-positive cells. The increase in $[Ca^{2+}]_i$ was reversibly suppressed by the specific voltage-gated sodium channel blocker, tetrodotoxin. Scale bar; 50 μm.

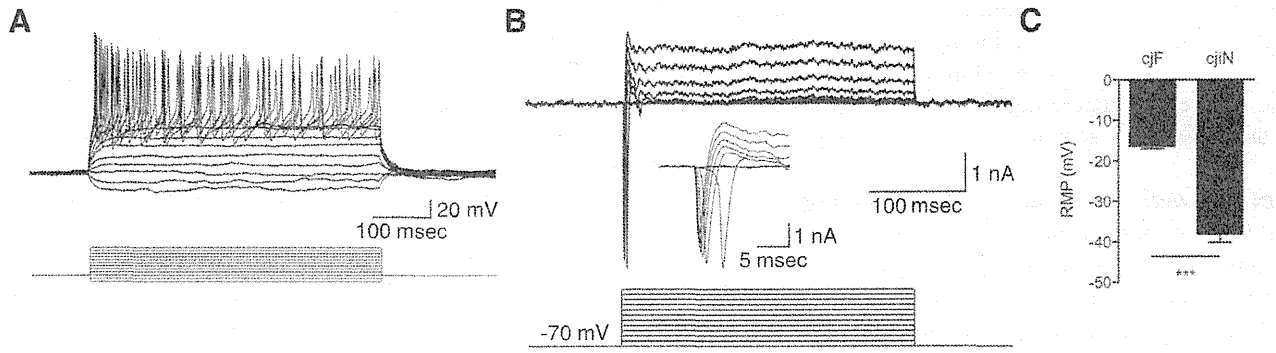

Figure 6 Neuronal electrophysiological property of cjiN cells. **(A)** cjiN cells elicited repetitive action potential by membrane depolarization in current-clamp mode. **(B)** cjiN cells showed both fast-activating and inactivating sodium currents and outward currents in voltage-clamp mode. **(C)** cjiN cells exhibited significantly lower resting membrane potentials than cjFs. $P^{***} < 0.001$ (Mann-Whitney *U*-test).

progenitor-like cell state, 5-bromodeoxyuridine (BrdU; 10 μM) was added to the media at 1, 3 or 5 div until 24 div (Figure 7A), and the percentage of double-positive cells for BrdU and MAP2 among the MAP2 single-positive cells was determined (Figure 7B, C). The result showed that while 85.3 ± 5.4% of MAP2-positive cells incorporated BrdU when treated from 1–24 div, only 30.1 ± 9.0% ($P^{**} < 0.01$) and 1.5 ± 1.5% ($P^{***} < 0.001$) of MAP2-positive cells incorporated BrdU when treated from 3–24 and 5–24 div, respectively (Figure 7C). This result indicates that most of the cells that were destined to be cjiN cells became postmitotic at the early phase of the reprogramming process, suggesting that cjiN induction is a direct process unless cells pass through a proliferative neural progenitor-like cell state, from which neuronal cells can be differentiated. In the present study, however, no Sox2-positive cells were found during 2–5 div, while MAP2-positive cells were present at 21 div (data not shown), indicating that the induction of neural progenitor-like cells is unlikely during 1-5 div. Therefore, these results show that cjiN cells are directly converted from cjFs without passing through proliferative neural progenitor cells.

Conclusions

In the present study, we established an *in vitro* method to convert common marmoset somatic cells into functional neuronal (i.e. cjiN) cells. The majority of the cjiN cells were

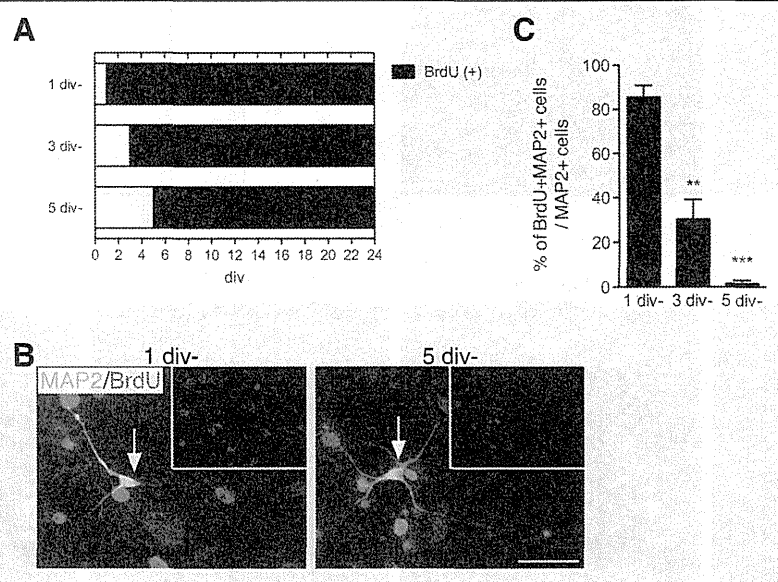

Figure 7 Cells destined to be cjiN cells became postmitotic at the early phase of the reprogramming process. **(A)** Time course for the BrdU incorporation experiment. BrdU (10 μM) was added into the culture medium at 1, 3 or 5 div until cells were fixed at 24 div. **(B, C)** Immunocytochemistry against MAP2 and BrdU revealed that when cells were treated with BrdU at 1 div until 24 div, 85.2 ± 5.4% of cjiN cells were BrdU + MAP2+, while when treated at 3 or 5 div until 24 div, only 30.1 ± 9.0% or 1.5 ± 1.5% of cjiN cells were BrdU + MAP2+, respectively, showing that the cjFs became postmitotic soon after transgene expression. $P^{***} < 0.001$ $P^{**} < 0.01$. Scale bar; 50 μm.

vGlut1-positive excitatory neuronal cells and expressed the neuronal marker genes: *TUBB3*, *DCX*, *MAP2*, *SYN1*, *VGLUT1*, *SCN1A*, *GRIN1* and *GRIA1*. Importantly, cjF-derived cjiN cells exhibited functional neuronal properties and responded to exogenous stimulation. Overall, these findings suggest that direct conversion technology may be beneficial in rapid and robust screening of neuronal phenotypes of transgenic common marmoset models of human diseases and analyzing underlying molecular mechanisms of diseases.

Methods

Animals

All animal experiments were approved by the Institutional Animal Care and Use Committee of the Central Institute for Experimental Animals (CIEA), and was performed in accordance with CIEA and Keio University guidelines.

Cell culture

Common marmoset embryonic fibroblasts, NIH3T3 cells and 293T cells were cultured in Dulbecco's modified Eagle's medium supplemented with 10% fetal bovine serum, 100 U/mL of penicillin and 100 μg/mL of streptomycin (10% FP medium) at 37°C with 5% CO_2 incubation.

Molecular cloning and lentivirus production

cDNA entry clone of human *ASCL1* [GenBank: NM_004316] was purchased from DNAFORM (clone ID: 100006383, Japan). cDNAs of human *BRN2* [GenBank: NM_0056 04.3], *MYT1L* [GenBank: NM_015025.2] and *NEUROD1* [GenBank: NM_002500.4] were cloned into pENTR-D-TOPO vector (Invitrogen, USA). Then cDNAs were inserted into a self-inactivation human immunodeficiency virus-1-based lentivirus construct, CSIV-TRE-RfA (CSIV-TRE-RfA-CMV-KT was kindly provided by Dr. Hiroyuki Miyoshi (RIKEN BRC, Japan), and then modified by Dr. Takuji Maeda (Nagoya University, Japan)), by LR reaction (Invitrogen, USA). Similarly, reverse tetracycline transactivator (rtTA) gene was inserted into CSII-EF1α-RfA-TK-HygR construct [27]. The human synapsin I reporter constructs, pCSC-hSynI-GFP [16] and pHIV7-hSynI-DsRed [18], were kindly provided by Dr. Fred H. Gage, Salk Institute, USA, and Dr. Alysson R. Muotri, University of California, USA, respectively. Besides, CSIV-hSynI-GFP-IRES2-NeoR and CSIV-hSynI-DsRed-IRES2-NeoR were constructed in-house. These reporters were constructed using CSIV-TRE-RfA-CMV-KT, pCSC-hSynI-GFP, pHIV7-hSynI-DsRed and pIRESneo3 (Clontech, USA) with PCR- and restriction enzyme-based method. For lentivirus production, 293T cells were transfected with lentivirus plasmid, pCAG-HIVgp and pCMV-VSV-G-RSV-Rev [28] (kindly provided by Dr. Hiroyuki Miyoshi, RIKEN BRC, Japan). After 16-20 h, supernatant was replaced by fresh media followed by 48-72 h incubation. The virus containing media were then collected and 0.45 μm-filterated followed by ultracentrifugation. The concentrated virus was suspended in PBS and used in subsequent experiments.

Induction of common marmoset iN cells

Common marmoset embryonic fibroblasts were seeded directly on culture ware at 1×10^4 cells/cm^2. Twenty-four hours later, the cells were infected with lentivirus in 10% FP media containing polybrene (8 μg/mL) (Sigma-Aldrich, USA). After 16–20 h in media containing lentivirus, the cells were switched into fresh 10% FP medium containing doxycycline (dox) (2 μg/mL) to drive transgene expression. Procedures for experiments determining the sufficient concentration and duration of dox are shown in the main text. After 48 h in 10% FP media with dox, the media was replaced with dox-containing neural media composed of N2B27 media [20], brain-derived neurotrophic factor (BDNF) (10 ng/mL, R&D systems, USA) and neurotrophin-3 (NT-3) (10 ng/mL, R&D systems, USA). For calcium imaging, 8-(4-Chlorophenylthio) adenosine 3′, 5′-cyclic monophosphate (8-CPT, 100 μM, Sigma-Aldrich, USA), one of the cAMP analogs [29], was also supplemented to promote neuronal maturation. The media was changed every 2–3 days during culture period. BrdU incorporation assay was performed as previously described [9] incubating cells with BrdU (10 μM, BD, USA) until cells were fixed.

Immunocytochemistry

Cells were fixed with 4% paraformaldehyde for 15 minutes at room temperature and then processed for immunocytochemistry [13]. Samples were rinsed with PBS three times. Then, samples were incubated at 4°C overnight with the primary antibodies diluted in PBS containing 5% of fetal bovine serum and 0.3% Triton X-100. The primary antibodies used were as follows; Synaptophysin (1:50000, Millipore, USA), MAP2 (1:1000, Sigma-Aldrich, USA), MAP2 (1:500, Millipore, USA), vGlut1 (1:2000, Synaptic systems, Germany), GABA (1:1000, Sigma-Aldrich, USA), PSD95 (1:500, Millipore, USA), α-SMA (1:500, Sigma-Aldrich, USA), Sox2 (1:500, R&D, USA), Ascl1 (1:200, BD, USA), Brn2 (1:200, Santa Cruz, USA), Myt1L (1:500, Abcam, England) and NeuroD1 (1:500, Santa Cruz, USA). After three washes with PBS, samples were incubated with secondary antibodies conjugated with Alexa-488, Alexa-555 and Alexa-647 (Invitrogen, USA). Nuclei were counterstained with 4′, 6-diamidino-2-phenylindole (DAPI; 1:1000, Dojindo, Japan). After washing with PBS, samples were mounted on slides with FluorSave reagent (Calbiochem, Germany) and examined under a universal fluorescence microscope (Axioplan 2; Carl Zeiss, Germany). For anti-BrdU staining (1:500, Abcam, England), cells were treated with 1 N HCl in PBS for 30 minutes at